HHS Public Access

Author manuscript

J Bone Miner Res. Author manuscript; available in PMC 2023 March 01.

Published in final edited form as:

J Bone Miner Res. 2022 February ; 37(2): 285–302. doi:10.1002/jbmr.4468.

The glucocorticoid receptor in Osterix-expressing cells regulates bone mass, bone marrow adipose tissue, and systemic metabolism in female mice during aging

Jessica L. Pierce, PhD[1], **Anuj K. Sharma, BDS**[1], **Rachel L. Roberts, MS**[1], **Kanglun Yu, MD MS**[1], **Debra L. Irsik, PhD**[2,4], **Vivek Choudhary, PhD**[3], **Jennifer S. Dorn, BS**[1], **Husam Bensreti, BDS, MS**[1], **Reginald D. Benson Jr, BS.**[1], **Helen Kaiser, PhD**[1], **Andrew Khayrullin, BS**[1], **Colleen Davis, PhD**[1], **Chase J. Wehrle**[1], **Maribeth H. Johnson, MS**[2], **Wendy B. Bollag, PhD**[3,4], **Mark W. Hamrick, PhD**[1], **Xingming Shi, PhD**[2], **Carlos M. Isales, MD**[2], **Meghan E. McGee-Lawrence, PhD**[1,5,*]

[1]Department of Cellular Biology and Anatomy, Augusta University, Augusta, GA

[2]Department of Neuroscience and Regenerative Medicine, Augusta University, Augusta, GA

[3]Department of Physiology, Augusta University, Augusta, GA

[4]Charlie Norwood VA Medical Center, Augusta, GA

[5]Department of Orthopaedic Surgery, Augusta University, Augusta, GA

Abstract

Hallmarks of aging-associated osteoporosis include bone loss, bone marrow adipose tissue (BMAT) expansion, and impaired osteoblast function. Endogenous glucocorticoid levels increase with age, and elevated glucocorticoid signaling, associated with chronic stress and dysregulated metabolism, can have a deleterious effect on bone mass. Canonical glucocorticoid signaling through the glucocorticoid receptor (GR) was recently investigated as a mediator of osteoporosis during the stress of chronic caloric restriction. To address the role of the GR in an aging-associated osteoporotic phenotype, the current study utilized female GR conditional knockout (GR-CKO; $GR^{fl/fl}$:Osx-Cre+) mice and control littermates on the C57BL/6 background aged to 21 months and studied in comparison to young (3- and 6-month-old) mice. GR deficiency in Osx-expressing cells led to low bone mass and BMAT accumulation that persisted with aging. Surprisingly, however, GR-CKO mice also exhibited alterations in muscle mass (reduced %lean mass and soleus fiber size), accompanied by reduced voluntary physical activity, and also exhibited higher whole-body metabolic rate and elevated blood pressure. Moreover, increased lipid storage was observed in GR-CKO osteoblastic cultures in a glucocorticoid-dependent fashion despite genetic deletion of the GR, and could be reversed via pharmacological inhibition of the mineralocorticoid

*Corresponding Author: Meghan E. McGee-Lawrence, Ph.D., 1120 15th Street, Augusta, GA 30912, mmcgeelawrence@augusta.edu.

AUTHOR CONTRIBUTIONS

Study design: MEML and JLP. Study conduct: JLP, AKS, RLR, DLI, HB. Data collection: JLP, AKS, RLR, DLI, VC, HB, RDB, HK, AK. Data analysis: JLP, AKS, KY, DLI, JSD, HK, AK, CD, HB, CJW, MHJ, and MEML. Data interpretation: JLP, HB, DLI, MHJ, and MEML. Drafting manuscript: JLP and MEML. Revising manuscript content: JLP, DLI, WBB, XMS, and MEML. Approving final version of manuscript: JLP, AKS, RLR, KY, DLI, VC, JSD, HB, RDB, HK, AK, CD, CJW, MHJ, WBB, MWH, XMS, CMI, and MEML. JLP and MEML take responsibility for the integrity of the data analysis.

Disclosures: The authors state that they have no conflicts of interest.

receptor (MR). These findings provide evidence of a role for the GR (and possibly the MR) in facilitating healthy bone maintenance with aging in females. The effects of GR-deficient bone on whole-body physiology also demonstrate the importance of bone as an endocrine organ and suggest evidence for compensatory mechanisms that facilitate glucocorticoid signaling in the absence of osteoblastic GR function; these represent new avenues of research that may improve understanding of glucocorticoid signaling in bone towards the development of novel osteogenic agents.

Keywords

Aging; osteoblasts; osteoporosis; glucocorticoids; bone marrow adipose tissue (BMAT)

INTRODUCTION

The development of osteoporosis is linked to aging mechanisms and is characterized by decreased bone density, increased risk of fracture, and numerous injury-associated comorbidities [(1)]. There are many aging-related factors that contribute to the pathogenesis of osteoporosis, including estrogen decline, changes to epigenetic signatures, increased circulating glucocorticoids and inflammatory cytokines, reduced physical activity (disuse), and increased oxidative stress in osteogenic cells [(2)]. Because the relationships between these factors are complex, ongoing research aims to understand these mechanisms in order to improve therapeutic approaches to treating osteoporosis as well as develop effective preventative measures prior to disease onset.

The risk of osteoporotic fracture in patients is inversely associated with bone mineral density [(3)]. Dysregulated bone remodeling and concordant bone loss is driven not only by increased osteoclast bone resorption but also by impaired osteoblast function and decreased osteogenic commitment of the progenitor bone marrow stromal cell (BMSC) population [(4)]. More recently, osteoporosis has also been characterized as a metabolic disease of the bone, marked by increased bone marrow adipose tissue (BMAT) accumulation [(5–7)]. The relationship between BMAT and bone is complex and not fully understood. BMAT increases under conditions associated with low bone mass including disuse from spinal cord injury [(8)], high fat diet administration [(9)], exogenous glucocorticoid treatment [(10)], and aging [(11)], and yet several previous studies have demonstrated that BMAT may not be a causative factor for osteoporosis [(12–16)]. Bone marrow adipocytes serve as reservoirs for energy-rich fatty acids and help cultivate a microenvironment that supports osteogenic cells, but also secrete molecules that can compromise osteoblast function [(17–19)]. As bone marrow adipocytes and osteoblasts share a common progenitor cell, the lineage commitment patterns of BMSCs must be dynamic yet tightly regulated to enable bone to meet local bio-energetic demands, respond to nutrient and endocrine stimuli, and orchestrate systemic physiological processes through tissue crosstalk mechanisms [(20)].

Glucocorticoids are mediators of stress responses and anti-inflammatory signaling throughout the body. Glucocorticoids are synthesized and secreted by the adrenal cortex as a product of the hypothalamic-pituitary-adrenal (HPA) axis, following distinct temporal

patterns that become dysregulated with aging [21–23]. Active glucocorticoids (cortisol in humans and corticosterone in mice) bind the glucocorticoid receptor (GR; encoded by the gene *Nr3c1*) within target tissues to drive downstream stress-response signaling cascades through receptor dimerization, translocation, and association with transcription factors and glucocorticoid response elements (GREs) [24–28]. An excess of circulating glucocorticoids (e.g., with Cushing's syndrome) can compromise bone mass by inhibiting osteoblast differentiation and inducing osteoblast and osteocyte apoptosis [29–31]. Additionally, exogenous glucocorticoid treatments for chronic inflammatory diseases contribute to the development of a secondary form of osteoporosis, glucocorticoid-induced osteoporosis [32].

Despite our increasing knowledge regarding the pathophysiology of glucocorticoid-induced osteoporosis in patients receiving anti-inflammatory therapies, endogenous glucocorticoids and the mechanisms by which they impact aging bone are not as well understood. We became interested in endogenous glucocorticoid signaling through our previous investigation of the role of the epigenetic regulator histone deacetylase 3 (Hdac3) in regulating bone maintenance and BMAT expansion [33]. Loss of Hdac3 in BMSC-derived osteoprogenitors caused increased expression of the endogenous glucocorticoid-activating enzyme *Hsd11b1* that was consistent with increased gene expression levels of *Hsd11b1* seen in aged WT osteoblasts [33]. Moreover, this change in either Hdac3-deficient or aging WT mice was associated with a phenomenon of *in vitro* osteoblastic lipid storage that was dependent on glucocorticoid signaling, as accumulation of lipids in the osteoblast cultures required the presence of the synthetic glucocorticoid dexamethasone (Dex) [33]. Conflicting evidence in the literature exists regarding the role of endogenous glucocorticoids in skeletal maintenance *in vivo*. Impairment in skeletal glucocorticoid signaling via transgenic overexpression of the glucocorticoid-inactivating enzyme *Hsd11b2* in osteocalcin-expressing mature osteoblasts was protective against glucocorticoid-induced bone loss and osteogenic cell apoptosis, implicating canonical glucocorticoid signaling as a potential mechanism by which excess glucocorticoids initiate bone loss [34]. This same *Hsd11b2*-transgenic model demonstrated protection against age-related bone loss in the spine [35]. However, a recent study overexpressing *Hsd11b2* in mature osteoblasts via the type 1 collagen promoter showed an opposite effect, where *Hsd11b2*-transgenic mice presented with a mild loss of trabecular bone in the spine [36]. Moreover, a mouse model of glucocorticoid receptor (GR) conditional deletion in osteoblasts (Runx2-Cre) further demonstrated that the GR mediates the glucocorticoid-induced loss of bone mass, although young GR-CKO_{Runx2} mice exhibited a significant decrease in bone density in the spine that was due in part to impaired osteoblast differentiation [37]. Recently, we assessed the role of the GR in Osterix-expressing osteoprogenitors in a model of osteoporosis induced by metabolic stress (chronic caloric restriction) with the initial expectation that loss of GR function would be protective against caloric restriction-induced osteoporosis in young mice. However, we found that GR deficiency surprisingly accentuated the BMAT accumulation and bone loss observed with caloric restriction [38].

In the current study, we sought to utilize the widely applicable stress of biological aging as a model for excess circulating glucocorticoids to test whether canonical glucocorticoid signaling mediated by the GR affects the pathophysiology of osteoporosis. Based on our earlier work [38], we hypothesized that GR-deficient mice would demonstrate exacerbated

bone loss and increased BMAT with age as compared to control littermates. While these trends were observed, we were surprised to find that GR deficiency in aged bone also was associated with alterations in muscle mass and systemic metabolic changes, raising the possibility that GR function in the skeleton may affect extra-skeletal physiology through tissue crosstalk mechanisms.

MATERIALS AND METHODS

Animal models

All animals used for the current study were female mice on a C57BL/6 background. For this aging model, female mice were chosen for study for three reasons: 1) to best compare against our earlier studies with GR-deficient mice and caloric restriction (also conducted in females) [38], 2) because females exhibit a greater risk for developing osteoporosis during aging, and 3) because female mice are easily housed in groups to facilitate efficient long-term research studies [39,40]. Mice were group housed in an accredited facility and maintained on a 12-hour light/dark cycle, and the research was conducted according to guidelines provided by the National Institutes of Health (NIH) and under protocols approved by the Augusta University Institutional Animal Care and Use Committee (IACUC). Mice were maintained on a standard rodent diet (Teklad 8904) and allowed food and water *ad libitum* unless otherwise stated for an experiment. Mice with *loxp* sites flanking exon 2 of the GR were crossed with Osx-Cre+ mice for several generations as described in our previous study to generate GR-conditional knockout (GR-CKO; $GR^{fl/fl}$:Osx-Cre+) mice along with wild-type (GR-WT; $GR^{fl/fl}$:Osx-Cre−) littermates [38]. This GR-floxed allele deletes ~50% of the mature GR protein, encompassing the translation start site and the tau 1 transactivation domain, and has previously been shown to effectively disrupt GR action [41–43]. In our earlier publication, we demonstrated significant knockdown of GR mRNA in this mouse model in isolated BMSC-derived osteoprogenitor cells via semi-quantitative real-time PCR and in tissue sections via immunohistochemistry [38]. Because the skeletal phenotype and body mass deficiency of Osx-Cre+ control mice largely resolves by 12 weeks of age [44,45], one group of animals used in this study were maintained without doxycycline to allow for constitutive developmental expression of Cre in Osx-expressing cells. These mice are hereafter referred to as the “constitutive GR-conditional knockout” (constitutive GR-CKO) model. However, to address known concerns with the Osx-Cre driver [44–47], we also employed the Tet-OFF feature of the Osx-Cre as described previously [33,48], where an additional subset of mice was maintained on doxycycline chow (625 mg/kg; Envigo Teklad) until 3 months of age to suppress Cre activation followed by normal chow for 3 months to induce Cre activation and genetic deletion of the GR prior to sacrifice at 6 months of age. These mice are hereafter referred to as the “adult onset GR-CKO” model and were utilized to assess the skeletal phenotype of adult GR-CKO mice in the absence of potential confounding effects of Osx-Cre expression and GR deficiency during early development. Mice were sacrificed under isoflurane anesthesia to minimize confounding effects of stress during sacrifice [49], and tissues were collected at sacrifice.

Body composition analyses

Dual energy X-ray absorptiometry (DXA; Kubtec Digimus, KUB Technologies, Stratford, CT, USA) measurements were performed on 6- and 21-month-old mice at sacrifice. Bone mineral content (BMC, grams) and bone mineral density (BMD, g/cm^2) were calculated for the whole body (excluding the head and ear tag) and regions-of-interest (ROI) using the manufacturer's analysis software (Kubtec Digimus). Femur midshaft ROI measurements (BMC, BMD) were defined in the middle third of the femur in whole mouse X-ray images. Measurements of whole-body percent lean and percent fat mass were also calculated using the Digimus software. Body composition measurements for this instrument were validated against nuclear magnetic resonance (NMR) imaging, demonstrating excellent correlation between the two techniques (please see Supplemental Methods and Supplemental Figure S2).

Muscle fiber size measurements

Soleus (slow twitch) and extensor digitorum longus (EDL; fast twitch) muscles were harvested from hindlimbs of 3-, 6- and 21-month-old mice at sacrifice. Tissues were either embedded in optimal cutting temperature (O.C.T.; Fisher Scientific) medium and sectioned by cryostat or were fixed in 10% neutral-buffered formalin followed by paraffin embedding and microtome sectioning (Leica Biosystems, Buffalo Grove, IL, USA). Muscle tissue sections were stained using Masson's trichrome and images were captured using a 20X microscope objective. Analyses of muscle fiber size were performed using ImageJ software by quantifying muscle fiber area in a 10,000 μm^2 grid across 20 sample sections from each muscle.

Bone histology and histomorphometry

The 3- and 21-month-old mice received dual injections of calcein (10 mg/kg body mass) prior to sacrifice to label mineralizing bone surfaces. Femora and tibiae were harvested and fixed in 10% neutral-buffered formalin for 48 hours. Femora were scanned by micro-computed tomography (microCT; 10.5 μm voxel size) using a Skyscan 1272 system (Bruker) with settings of 70kV and 300 ms for analyses of cortical and trabecular bone architecture. The cortical bone region of interest was 50 slices in length, beginning 500 slices (scaled to bone length) proximal to the distal femoral metaphysis growth plate. The trabecular bone region of interest was 50 slices in length, beginning adjacent to the distal femoral metaphysis growth plate. Bone architectural and density parameters were calculated using the manufacturer's software as previously described [(38)]. After microCT scanning, bones were embedded in methylmethacrylate and sectioned for trabecular bone dynamic histomorphometry measurements in the distal femoral metaphysis as previously described [(38)].

For analyses of BMAT, osteoblast surface, and osteoclast surface, tibiae from 6- and 21-month-old mice were decalcified in 15% EDTA for two weeks followed by paraffin embedding and sectioning using a Leica Microtome (7 μm sections; Leica Biosystems, Buffalo Grove, IL, USA). Hematoxylin and eosin (H&E; Sigma-Aldrich #HHS16, #H110316) staining protocols were used to visualize and quantify BMAT and osteoblasts, and histology images were captured using an Olympus IX70 inverted microscope (Olympus

Corporation, Center Valley, PA, USA) with a camera attachment (Qicam; QImaging). Bone marrow adipocyte area fraction (Ad.Ar/M.Ar, %), adipocyte density (N.Ad/Ma.Ar #/mm^2), osteoblast number (N.Ob/B.Pm, #/mm), and osteoblast surface (Ob.S/BS, %) were quantified using Bioquant Osteo software (Bioquant Osteo, Nashville, TN). Osteoclast surface (Oc.S/BS, %) and osteoclast number (N.Oc/BS, #/mm) measurements were acquired following a tartrate-resistant acid phosphatase (TRAP; Sigma-Aldrich #386A)/fast green staining protocol and mounting with a xylene-based mounting medium. TRAP-stained sections were analyzed in the proximal tibia metaphyseal trabecular bone using Bioquant Osteo software. Images were captured with 10X (H&E) and 20X (TRAP) objectives.

Metabolic cage and voluntary wheel running experiments

A subset of 21-month-old GR-WT and GR-CKO mice were analyzed using the Comprehensive Laboratory Animal Monitoring System (CLAMS; Columbus Instruments, Columbus, OH USA). CLAMS cages were utilized to measure food consumption, respiratory exchange (O_2 consumption, CO_2 release), body heat, and voluntary ambulatory movements across x-, y-, and z-axes over a 5-day period. Body mass measurements were recorded at the start of the study to normalize the metabolic data. Data recorded during the first day in the CLAMS cages were excluded from analysis to account for animal adjustments to the novel environment. To further analyze voluntary physical activity, the same groups of GR mice were singly housed in individual Mouse Home Cage Running Wheel systems equipped with water and standard chow for a 5-day monitoring period (Columbus Instruments, Columbus, OH, USA).

For additional physiological measurements, 21-month-old mice were individually housed in metabolic cages (Lab Products, Inc.). Following an acclimation period, 24-hour urine samples were collected, and urine electrolytes were measured by atomic absorption (Perkin Elmer, Shelton OH). Conscious systolic blood pressure was measured by tail-cuff plethysmography (Visitech Systems) following training sessions and acclimation to the instrument. Mice were placed in the restraints on a heated (36°C) plate and allowed several minutes to relax prior to initiation of 10 practice measurements. Average systolic pressure and heart rate for each mouse were computed from up to 20 subsequent consecutive measurements.

Fasting glucose measurements

Measurements of blood glucose levels were conducted on 6- and 21-month-old mice fasted for 6 hours during the native resting period (6 a.m. – 6 p.m.). All animals were provided *ad libitum* access to water during the fasting period. Bleeding was initiated by tail nick using a 21-gauge needle, and blood glucose levels (mg/dl) were measured a minimum of two times per mouse using the Bayer Breeze2 handheld glucometer (Bayer AG, Leverkusen, Germany). The fasting glucose level for each mouse represents the average of the repeat measurements taken during the blood sample harvest. Animal handling and blood glucose measurements were kept to under 3 minutes per mouse to minimize any confounding effect of stress [(50)].

Serum analyses

Whole blood was obtained from 6- and 21-month-old mice by cardiac puncture at sacrifice followed by centrifugation in serum separator tubes (BD Microtainer #365967; Becton Dickinson, Franklin Lakes, NJ, USA) to obtain terminal serum samples. Serum corticosterone levels were quantified by ELISA (Abcam #ab108821, Cambridge, MA, USA) using a 100-fold dilution of mouse serum and provided protocols. An additional corticosterone ELISA was performed on sera harvested from timed, non-terminal blood draws obtained over the murine nocturnal active period (i.e., 6:00 p.m., 12:00 a.m., and 6:00 a.m.) in aged (21-month-old) GR mice; these timed blood draws were collected via tail nick as described above for fasting glucose measurements. Animal handling and blood collection procedures were kept to under 3 minutes per mouse to minimize any confounding effect of stress [50,51]. All ELISA plates were measured with a microplate reader (BioTek Synergy HT, Winooski, VT, USA) using Gen5 software and reading at the 450 nm wavelength. Serum data were normalized to calibrants and standards provided in the ELISA kits.

Gene expression analyses

Cortical bone samples were harvested and flushed with a syringe to remove the bone marrow. The bones were cut into 1–2 mm sections using a scalpel, and bone chips were partially digested by three incubation steps in collagenase type 1A solution (activity 300 U/mg) in a shaking incubator. Digested bone chips were washed with PBS to remove collagenase and frozen for later homogenization in TRIzol RNA lysis reagent (Thermo Fisher Scientific). Total RNA was isolated and reverse transcribed as previously described [38]. Expression levels of mRNA for the GR (official gene name: nuclear receptor subfamily 3, group C; *Nr3c1*) were quantified by subjecting cDNA to real-time PCR amplification (37.5 ng cDNA per 15 μL reaction volume reaction, run in triplicate) using a Bio-Rad CFX Connect system, SYBR green reagent (Quanta Biosciences #95054-500) and primers designed to bind within the floxed region of the GR exon 2. Gene expression levels were quantified using the comparative threshold cycle (2–ΔΔCt) method [33]. Glyceraldehyde-3-phosphate dehydrogenase (GAPDH) was used as the internal control (housekeeping gene) for normalization. Primer sequences (5’ - 3’) are as follows: GAPDH_F: GGGAAGCCCATCACCATCT; GAPDH_R: GCCTCACCCCATTTGATGTT; GR_F: CTCCCCCTGGTAGAGACGAA; GR_R: TCCCATGGACAGTGAAACGG.

BMSC isolation and primary cell culture

Primary bone marrow stromal cells (BMSC) were harvested from long bones (i.e., femora, tibiae, humeri) by syringe flush using basal cell culture medium: Minimum Essential Medium (MEM)-α (Gibco #12561-072; Thermo Fisher Scientific, Waltham, MA, USA) + 20% fetal bovine serum (FBS; Atlanta Biologicals #S11150H, Flowery Branch, GA, USA) + 1% antibiotic-antimycotic (Gibco #15240-062) + 1% MEM non-essential amino acids (Gibco #11140-050). Osteogenic induction (to obtain BMSC-derived osteoblasts; BMSC-OB) began at seeding (Day 0) using basal cell culture medium containing ascorbic acid (50 μg/ml; Sigma-Aldrich #A4544) and β-glycerophosphate (10 mM; Sigma-Aldrich #G9422). Unless otherwise specified, osteogenic induction medium also contained the synthetic exogenous glucocorticoid dexamethasone (Dex, 10^{-7} M; Sigma-Aldrich #D1756)

based on previous work including glucocorticoids in osteogenic induction cocktails [33,38,52]. To test the effects of GR and mineralocorticoid receptor blockade *in vitro*, mifepristone (RU-486; 10^{-6} M), spironolactone (10^{-6} M), or eplerenone (10^{-6}M) were included in the osteogenic induction media where indicated. Culture medium for primary cells was changed every 3 days. To visualize lipid storage, primary BMSC-derived osteoblasts were cultured for 21 days and fixed with 10% neutral-buffered formalin, then dehydrated and stained with a 60% Oil Red O solution (Sigma-Aldrich #O0625). Microscopic well images were acquired at 10X magnification using the EVOS Cell Imaging System (Thermo Fisher Scientific), and the number of Oil Red O-containing cells in each culture was quantified with Image J.

Statistical analyses

In vivo data were calculated using biological replicates (i.e., individual mice) from each experimental group; sample sizes are stated in each figure caption. When only two groups were compared (i.e., GR-WT vs. GR-CKO), Student's t-tests were utilized and statistical significance reported with 95% confidence ($p<0.05$). To simultaneously compare the effects of two independent variables (e.g., genotype and age, or genotype and time of day), statistical comparisons were made by Analysis of Variance (ANOVA) using JMP Pro 15 statistical analysis software (SAS Institute Inc., Cary, NC, USA). Tukey-Kramer post-hoc tests were conducted when significant ($p<0.05$) interaction effects were present to determine pairwise comparisons. For *in vitro* cell culture experiments, cells were pooled together (by respective experimental group), seeded into tissue culture plates for a minimum of three technical replicates (separate wells) per experiment, and repeated at least three times using different batches of mice (biological replicates). Groups were compared by t-test (2 groups) or ANOVA (3+ groups) depending on experimental design. Box plots in figures show median, quartiles, and outlier fences for each dataset, where outlier fences represent first quartile - 1.5*(interquartile range) and third quartile + 1.5*(interquartile range). Bar charts show mean and standard error.

RESULTS

Conditional deletion of the glucocorticoid receptor in osteoprogenitors

Previous work investigating the pathogenesis of osteoporosis in models of aging, chronic metabolic stress, and Hdac3 conditional deletion suggested a role for local glucocorticoid signaling in regulating bone loss and bone marrow adipogenesis [33,34,38,53]. As such, we sought to determine the effects of loss of GR function in Osx-expressing cells on an aging-associated osteoporotic phenotype. The efficacy of the knockdown was first established, in observing that gene expression levels of the GR were significantly reduced in cortical bone of 3-month-old constitutive GR conditional knockout (GR-CKO; blue boxes) mice as compared to wild-type (GR-WT; orange boxes) littermates (−89%, $p=0.033$; Figure 1A), consistent with our previous studies [38]. Expression of GR was also reduced in cortical bone of the 21-month-old constitutive GR-CKO mice (Supplemental Figure S2A). The constitutive GR-CKO mice showed indications of whole-body phenotypic differences, as 21-month-old GR-CKO animals were significantly smaller in terms of body mass than control (GR-WT) littermates (body mass: −21.6%, $p<0.0001$), although 3- and 6-month GR-WT and GR-CKO mice were more comparable in size and not significantly different

from one another (p>0.587; Figure 1B). To eliminate possible confounding effects of the Cre recombinase expression on phenotypic differences in the current study, the Tet-OFF feature of the Osx-Cre system was also utilized. Female GR-CKO mice and control littermates were maintained on a doxycycline-containing diet until 3 months of age to delay Cre-mediated recombination in Osx-expressing cells until the rapid phase of skeletal growth had subsided. While on doxycycline, cortical bone GR gene expression levels were not different between GR-WT and GR-CKO mice (p=0.819; Figure 1C). However, when doxycycline-treated GR-CKO mice were returned to a regular diet for 3 additional months to allow Osx-Cre expression, a significant reduction in GR expression was again detected in cortical bone of these adult-onset GR-CKO mice (p=0.024; Figure 1D). The adult onset GR-CKO and GR-WT littermates were not different in size (Figure 1E). In accordance with our previous report using GR-CKO mice [38], these data provide validation of the conditional deletion of the GR in bone (and osteoprogenitor cells) that serves as a foundation for the current study.

GR deficiency in Osx-expressing cells induced bone loss

Assessments by DXA (Kubtec Digimus) at 6- and 21-months of age did not show differences in whole-body bone mineral density (BMD; $p_{genotype}$=0.266; Figure 2A) or whole body bone mineral content (BMC; $p_{genotype}$=0.495; Figure 2B) between constitutive GR-WT and GR-CKO mice. Aging affected whole-body DXA parameters similarly between these GR-WT and GR-CKO animals, such that a trend of increased whole body BMD and BMC was observed with skeletal maturation (BMD p_{age}=0.040, Figure 2B; BMC p_{age} = 0.074, Figure 2C) but was not different between genotypes. Analyses of the femur midshaft region-of-interest in these DXA datasets indicated that loss of GR function in osteoprogenitors did not affect femur midshaft BMD ($p_{genotype}$ = 0.773; Figure 2C) but caused a decrease in cortical bone mineral content ($p_{genotype}$=0.0005; Figure 2D), consistent with a smaller body size (Figure 1B). Femur midshaft BMD was unaffected by age in either genotype, although femur BMC increased with age (p_{age} = 0.004, Figure 2D).

Bone properties were further interrogated by higher resolution microCT measurements in 3- and 21-month-old mice. Although lower-resolution DXA analyses failed to demonstrate differences in 2-dimensional femoral midshaft BMD (g/cm^2) between genotypes or ages, cortical bone tissue mineral density as measured by microCT (mg/cm^3) was lower in the constitutive GR-CKO as compared to GR-WT littermates, and increased between 3- and 21 months of age in both genotypes (Table 1). Cortical bone geometrical properties tended to increase (rather than decrease) between 3 and 21 months of age in the GR-WT mice (p_{age} <0.05 for most properties, Table 1), suggesting that the 3-month-old GR-WT mice used for these microCT analyses were still growing at the time of sacrifice. In contrast, age-related changes between 3- and 21-months of age were blunted in the constitutive GR-CKO mice ($p_{genotype*age}$ <0.05 for most properties), suggesting impaired bone growth during skeletal maturation consistent with a reduced body size (Figure 1B). Most cortical bone geometrical properties including tissue area, bone area, marrow cavity area, moments of inertia, and cortical thickness were similar between constitutive GR-CKO mice and their GR-WT littermates at 3 months of age, but smaller in constitutive GR-CKO mice as compared to GR-WT littermates at 21 months of age (Table 1; note that interaction effects approached significance for marrow cavity area and cortical bone thickness). Cortical

bone area and cortical bone thickness were also reduced in the adult-onset GR-CKO mice as compared to their WT littermates (Table 2), even though body mass was comparable between genotypes in this model (Figure 1E). Other cortical bone properties were not different between genotypes in the adult-onset GR-CKO model (Table 2).

In the trabecular bone of the distal femoral metaphysis, a strong age-related phenotype of trabecular bone loss between 3- and 21 months of age was observed across both genotypes in the constitutive GR-CKO model, validating the expected trends for an aging model ($p_{age} < 0.019$ for all properties, Table 1). Constitutive GR-CKO mice demonstrated strong trends for reduced trabecular bone volume fraction ($p_{genotype}=0.050$), trabecular thickness ($p_{genotype}=0.078$), and trabecular number ($p_{genotype}=0.052$), and showed a significant increase in trabecular separation ($p_{genotype}=0.022$) as compared to GR-WT littermates (Table 1) across both ages studied. Importantly, evidence of reduced trabecular bone mass was also evident in the adult-onset GR-CKO mice as compared to littermate controls. Adult-onset GR-CKO mice demonstrated significant reductions in trabecular BV/TV (p=0.0007) and trabecular thickness (p=0.011) as compared to WT littermates following delayed conditional deletion of the GR (Table 2). Together, these data suggest that loss of GR function in Osx-expressing cells negatively impacts trabecular and cortical bone mass.

We previously reported that the low bone mass phenotype of GR-CKO mice is attributable to decreased bone formation activity rather than to excessive bone resorption, as serum markers of both bone formation (P1NP) and bone resorption (TRAcP5b) were reduced in constitutive GR-CKO mice compared to GR-WT littermates [38]. Surprisingly, histological metrics of trabcular bone remdeling including osteoblast number (N.Ob/BS; Figure 3A–B), osteoblast surface (Ob.S/BS; Figure 3C), osteoclast number (N.Oc/BS; Figure 3D–E) and osteoclast surface (Oc.S/BS; Figure 3F) were not different between genotypes ($p_{genotype}\geq0.139$) or age groups ($p_{agee}\geq0.117$) in the current study; however, these trends may have been impacted by the low amount of remodeling activity and trabecular bone found in the proximal tibia at the ages studied. Dynamic histomorphometry measurements of trabecular bone mineralizing surface in 3- and 21-month-old mice demonstrated reduced bone formation activity in GR-CKO mice ($p_{genotype} = 0.045$, Fig 3G–H). Mineral apposition rate and bone formation rate were both reduced with age, but unaffected by genotype (Figure 3G–H). The reduced mineralizing surface measurements in GR-CKO mice observed here, consistent with our previous findings of reduced mineralizing surface and circulating P1NP levels in this GR-CKO model [38], suggest that the low bone mass phenotype of the GR-CKO mice is primarily attributable to impaired bone formation.

GR-CKO mice developed high BMAT

Given the increased marrow adiposity phenotype of GR-deficient bone in our previous caloric restriction study [38], a high BMAT phenotype in GR-CKO bone in response to the stress of aging was anticipated. This idea was confirmed in our histological analyses of 6-month and 21-month-old constitutive GR-WT and GR-CKO tibiae (Figure 4A). Conditional deletion of the GR in Osx-expressing cells tended to increase both BMAT area fraction (Figure 4A–B) and BMAT density (Figure 4C) as compared to GR-WT littermates. Consistent with the current knowledge on aging-associated BMAT expansion [5,54], aging

also tended to increased BMAT in both GR-WT and GR-CKO mice (p_{age}<0.067). An interaction effect of genotype and age was not observed in the context of BMAT accumulation (Ad.Ar/M.Ar $p_{genotype*age}$=0.920, N.Ad/M.Ar $p_{genotype*age}$=0.822; Figure 4B–C), suggesting that constitutive GR-CKO mice undergo aberrant marrow adipogenesis at younger ages that persists throughout their lifespan. Importantly, analyses of tibiae from the doxycycline-treated adult-onset GR-CKO mice further confirmed the effects of GR deficiency on the BMAT phenotype, as adipocyte area fraction and adipocyte density were significantly increased following loss of GR function in this model (p=0.04 and p=0.03, respectively; Figure 4D–E). These data suggest the potential importance of proper GR function in bone marrow progenitor cells for maintaining the balance between osteogenesis and adipogenesis, however since the Osx-Cre shows activity in bone marrow adipocytes [46], loss of GR expression in committed bone marrow adipocytes may have directly contributed to the increased BMAT aspect of the GR-CKO phenotype.

GR-CKO in Osx-expressing cells induced changes in muscle mass and reduced physical activity

Bone is an active endocrine organ that engages in tissue crosstalk and metabolic homeostasis throughout the body [20]. In accordance with this concept, constitutive conditional deletion of the glucocorticoid receptor in bone was associated with changes in various aspects of whole-body physiology. The constitutive GR-CKO mice demonstrated a mild but significant decrease in whole body percent lean mass ($p_{genotype}$=0.002, Figure 5A) and increase in whole body percent fat mass ($p_{genotype}$=0.010; Figure 5B) in DXA body composition analyses, with no interaction effect between age and genotype, however, we note that this effect was not seen in an additional group of female animals analyzed by either DXA or nuclear magnetic resonance (NMR) at 12 months of age (Supplemental Figure S1). Consistent with the reduction in percent lean mass, the constitutive GR-CKO mice also demonstrated a significant reduction in muscle fiber size in the predominantly slow-twitch soleus muscle compared to GR-WT littermates ($p_{genotype}$=0.006; Figure 5C). Muscle fiber size remained unchanged in the primarily fast-twitch extensor digitorum longus (EDL) muscle ($p_{genotype}$=0.967; Figure 5D), suggesting possible differences in fiber type affected by GR function in Osx-expressing cells. Interestingly, however, while quadriceps mass tended to be lower in constitutive GR-CKO animals (consistent with their smaller body mass), quadriceps mass normalized to body mass was actually increased in the constitutive GR-CKO animals (Figure 5E–F). Given the stronger skeletal and BMAT phenotype of the aged constitutive GR-CKO animals, the 21-month-old mice were subjected to further analysis in metabolic cages. Quantification of voluntary movement suggested that the decreased muscle mass in constitutive GR-CKO mice was associated with reduced physical activity. CLAMS measurements of cage ambulatory activity in the 21-month-old mice showed a significant reduction in movement across the x- ($p_{genotype}$=0.036; Figure 5G) and y-axes ($p_{genotype}$=0.041; Figure 5H); rearing activity in the z-plane was not affected ($p_{genotype}$=0.379; Figure 5I). These measurements were validated with a second method of assessing voluntary activity, with 21-month-old constitutive GR-CKO animals exhibiting a strong trend for reduced voluntary wheel running activity (p=0.060; Figure 5J) as compared to age-matched GR-WT animals. Circadian patterns of physical activity were maintained in the GR-CKO mice, as cage ambulatory activity increased during the active nocturnal

period as compared to the daytime resting period ($p \leq 0.021$), as expected, with no differences between GR-WT and GR-CKO mice ($p_{genotype \times time\ interaction} \geq 0.702$) (Figure 5G–I). Taken together, these data suggest that GR-insufficiency in Osx-expressing cells may impact the function of skeletal muscle.

GR-CKO in Osx-expressing cells altered systemic metabolism and homeostasis

CLAMS measurements of metabolic parameters also gave insights into the effects of constitutive GR deletion in Osx-expressing cells on energy homeostasis. Interestingly, oxygen consumption (VO_2, mL/kg/hr; Figure 6A) and carbon dioxide production (VCO_2, mL/kg/hr; Figure 6B) were both significantly higher in 21-month-old constitutive GR-CKO mice ($p_{genotype} \leq 0.003$) as compared to age-matched WT controls, but the respiratory exchange ratio was not different in GR-WT versus GR-CKO animals ($p_{genotype} = 0.436$; Figure 6C), suggesting no differences in the metabolism of carbohydrates versus fat between groups. Metabolic rate (kcal body heat/kg bodyweight/hr), on the other hand, was 10.8% higher in GR-CKO mice ($p = 0.003$; Figure 6D) compared to control animals during the 12-hour dark cycle. There were no differences in food consumption despite the increased metabolic parameters in GR-CKO mice (Supplemental Figure S3).

Conditional deletion of Hdac3 in Osx-expressing cells impacted whole-body metabolism and insulin sensitivity, and imparted a protective role against high fat diet-induced metabolic dysfunction [55,56]. Because conditional deletion of GR in Osx-expressing cells recapitulated similar bone mass and BMAT phenotypes as those observed in the Hdac3-deficient model [33,38], we investigated whether systemic homeostasis was affected to explore possible connections between metabolic dysfunction and the BMAT phenotype observed in this model. Measurements of fasting blood glucose revealed a trend for an interaction effect of genotype and age ($p = 0.062$; Figure 6E), with 6-month-old constitutive GR-CKO mice exhibiting a trend for lower fasting blood glucose levels compared to age-matched GR-WT mice while fasting glucose levels were comparable in 21-month-old GR-WT and GR-CKO animals ($p = 0.566$). Additionally, systolic blood pressure measurements in 21-month-old mice showed that constitutive GR-CKO animals developed elevated systolic blood pressure ($p = 0.011$; Figure 6F), although there were no changes in heart rate ($p = 0.325$, data not shown) between groups. A significant ($p = 0.0002$) decrease in urine sodium excretion in 21-month-old constitutive GR-CKO mice compared to GR-WT littermates was observed, suggesting the possibility of sodium retention that may affect blood pressure and related physiological measurements (Figure 6G); kidney weight was not affected ($p = 0.584$; Figure 6H). Taken together, these data suggested loss of the GR in Osx-expressing cells may cause changes to metabolic homeostasis, but the underlying mechanisms contributing to these phenotypes remain unclear.

Given the direct relationships between whole-body glucocorticoid signaling and the stress of aging [21], we sought to measure potential changes to adrenal gland physiology and circulating glucocorticoids. Total adrenal mass (normalized to body mass) was significantly higher in the constitutive GR-CKO animals ($p_{genotype} = 0.015$; Figure 7A), notable particualrly in the 21-month-old GR-CKO mice as compared to GR-WT littermates (24% increase in adrenal mass in old GR-CKO compared to old GR-WT). We previously

reported increased circulating corticosterone levels in constitutive GR-CKO mice during a stressed state of caloric restriction [38]. However, there were no differences in corticosterone levels in terminal serum samples between groups in the current study (Figure 7B). To definitively determine whether there were differences in corticosterone levels between genotypes in the aged mice, we performed non-terminal blood draws across the nocturnal active period for further analysis. Timepoint-specific serum corticosterone quantification showed a peak in the circulating hormone levels at the start of the nocturnal active period (around 6:00 p.m.) that gradually decreased over time (Figure 7C), which was consistent with established literature on the circadian variation of serum glucocorticoid levels in mice [22]. At the peak corticosterone timepoint of 6:00 p.m., serum levels of the hormone trended higher in constitutive GR-CKO mice as compared to GR-WT mice, but this increase did not reach statistical significance ($p=0.11$). Taken together, these data suggest that GR deficiency in Osx-expressing cells might induce an adrenal stress response, although further analyses of the specific downstream glucocorticoid signaling factors at play are needed to determine the mechanistic relationships.

GR-expression in non-skeletal tissues

The Osx-Cre has documented off-target effects outside the skeleton [46]. Although previous studies found no recombination induced by the Osx-Cre in extra-skeletal tissues including liver, adrenal glands, skeletal muscle, or white adipocytes [46], we sought to determine whether GR expression was affected outside of the skeleton in the 21-month-old mice as a possible explanation for the integrative physiological phenotype we observed. As a positive control, de-marrowed cortical bone shafts from the constitutive GR-CKO mice demonstrated reduced GR expression, as expected from our studies with younger animals (Supplemetnal Figure S2A). Interestingly, GR expression tended to be increased in key metabolic tissues including the gonadal white fat pad (Supplemental Figure S2B), the quadriceps muscle (Supplemental Figure S2C) and the liver (Supplemental Figure S2D) as compared to age-matched GR-WT mice. Therefore, although the Osx-Cre maintained its reported specificity in our 21-month-old mice [46], it is possible that compensatory up-regulation of GR outside of the skeleton could have contributed to the integrative physiology phenotype observed in these animals.

Loss of GR function in Osx-expressing cells may exacerbate glucocorticoid-driven lipid accumulation

We previously demonstrated that glucocorticoid-dependent osteoblastic lipid storage was observed in BMSC-derived osteoblasts from Hdac3-CKO and aged WT mice, suggesting that this mechanism may contribute to increased BMAT accumulation in these models [33]. In the current study, we tested whether deletion of the GR in Osx-expressing osteoprogenitors would be sufficient to negate this phenomenon. Surprisingly, GR-CKO BMSC-derived osteoblasts accumulated significantly more lipid droplets (Oil Red O+) than GR-WT cells when cultured in osteogenic induction medium containing the exogenous glucocorticoid dexamethasone (Figure 8). In particular, GR-CKO osteoblasts harvested from either constitutive GR-CKO or adult-onset GR-CKO mice consistently demonstrated an increased propensity to store lipid droplets compared to GR-WT controls across several independent batches of mice (i.e., independent biological replicates) (Figure 8A, 8D).

While BMSC cultures were only available from one cohort of mice used for aging studies with constitutive expression of Osx-Cre, increased lipid droplet storage was also observed in these GR-CKO osteoblasts as well, particularly in cells isolated from the aged animals (Figure 8A). To further assess whether *in vitro* GR inhibition would normalize the lipid-storing phenotypes between genotypes, an additional set of BMSC-derived osteoblast cultures were treated with the GR antagonist RU486. In this culture condition, osteoblastic lipid storage was robust in both GR-WT and GR-CKO cells at any age (Figure 8B, 8D), possibly due to a more complete inhibition of the GR in both cell types following pharmacological treatment. Thus, it is possible that the phenomenon of glucocorticoid-induced lipid storage we have observed here and previously [33] does not require signaling through the glucocorticoid receptor. Glucocorticoids are also known to bind and activate the mineralocorticoid receptor (MR), and to act on downstream response elements in bone through this pathway [57]; therefore, we also tested the effects of MR blockade with the MR inhibitors spironolactone or eplerenone. MR antagonism rescued the excess glucocorticoid-induced lipid droplet accumulation characteristic of GR-insufficient cultures (Figure 8C, 8D). Taken together, these data suggest that glucocorticoids mediate osteoblastic lipid storage and subsequent osteoblastic dysfunction, but may do so via signaling through the MR rather than the GR.

Loss of GR function in osteoprogenitors altered osteoblastic bioenergetics

To better understand the mechanisms involved in the GR-CKO bone phenotype, *in vitro* analyses of cellular bioenergetics were conducted on BMSC-derived osteoblasts from one cohort of 6- and 21-month-old constitutive GR-WT and GR-CKO mice. Seahorse extracellular flux analyses were performed using the Cellular Energy Phenotype test to measure rates of mitochondrial respiration and glycolysis. However, based on our previous experience with this assay [58], cells from all mice within each group were pooled together to accommodate the necessary number of technical replicates needed, thus, reducing our biological replicate sample size to n=1 for this experiment. Therefore, these results should be considered as preliminary, and are presented as a supplemental figure. Extracellular acidification rate, representing glycolytic activity, and oxygen consumption rate, representing oxidative phosphorylation were significantly higher in GR-CKO cells across age groups ($p<0.0001$ and $p=0.003$, respectively) under stressed conditions (Supplemental Figure S3A–C). Additionally, oxygen consumption rates increased with aging ($p=0.009$), consistent with the energy metabolism of maturing osteoblasts but also with a propensity for BMSC to undergo adipogenesis [59–61]. As a result of these measurements, GR-CKO osteoblasts were assigned a highly energetic metabolic profile (Figure S3A), as compared to GR-WT cells, which increased with aging. Together, these results suggest that the bone phenotypes induced by loss of GR function in Osx-expressing cells may be influenced by increased osteoblast bioenergetics and substrate metabolism. However, our interpretations of these findings are limited by a lack of biological replicates, and further metabolic analyses are needed to elucidate the effects of GR deficiency on osteoblast function.

DISCUSSION

The current study initially sought to determine whether GR function in Osx-expressing cells is required to mediate the harmful effects of aging-associated alterations in glucocorticoid signaling on bone mass and BMAT accumulation. In light of our earlier study [38], we hypothesized that GR-deficient mice would experience exacerbated bone loss with age as compared to control littermates, and indeed, GR-CKO mice demonstrated a significant reduction in both cortical and trabecular bone as compared to GR-WT controls. The cortical bone phenotype of the constitutive GR-CKO knockout mice was particularly pronounced at 21 months of age, as evidenced by a significant interaction between genotype and age for most cortical bone properties in this model (Table 1). As cortical bone is substantially influenced by body mass in mice [62], and body mass was decreased in the 21-month-old constitutive GR-CKO animals, it is difficult to separate the direct influence of loss of GR function in bone from reduced body mass in the causation of this phenotype. However, decreased cortical bone area and cortical bone thickness were also observed in the adult-onset GR-CKO mice, which were similar in size to their GR-WT littermates, at 6 months of age. Furthermore, it has been reported that body mass does not have an independent effect on trabecular bone in the distal femur of mice [62], and both the constitutive and adult-onset GR-CKO mice presented with decreased trabecular bone mass compared to WT control littermates at all ages studied. Together, these data provide stronger support for the importance of GR in maintenance of both cortical and trabecular bone mass, demonstrating that endogenous glucocorticoid signaling through the GR in Osx-expressing cells is necessary for the maintenance of bone mass with aging.

The role of glucocorticoid signaling in the pathophysiology of osteoporotic bone is of increasing interest in the field. Similar to our findings, it was previously reported that conditional deletion of the GR in Runx2-expressing osteoblasts reduced trabecular bone mass in the spine of young mice [37]. However, loss of osteoblastic GR function in these mice protected against the decreased bone formation and reduced osteocyte and osteoblast numbers that result from exogenous, therapeutic glucocorticoid administration. Another study demonstrated that the disruption of glucocorticoid signaling via overexpression of the glucocorticoid-inactivating enzyme Hsd11b2 in osteocalcin-expressing osteoblasts protected against glucocorticoid-induced bone loss *in vivo*, while conditional expression of Hsd11b2 in glucocorticoid-treated MLO-Y4 cells reduced osteocyte apoptosis *in vitro* [34]. A model of Hsd11b2 overexpression in osteoblasts and osteocytes ($HSD2^{OB/OCY}$-tg) also exhibited significant effects in peripheral adipose tissues by protecting against aging-related obesity and insulin resistance [63]. Despite this, there were minimal effects of Hsd11b2 overexpression on skeletal mass, and the effects on BMAT were not addressed in any of the previous studies mentioned above. Thus, the current study represents a novel investigation into the role of receptor-mediated glucocorticoid signaling in Osx-expressing cells on bone phenotypes in an aging model.

An interesting phenotype observed in both our constitutive and adult-onset GR-CKO models was BMAT accumulation, where GR conditional deletion in Osx-expressing cells increased adipocyte area fraction and adipocyte number in the bone marrow. It is possible that the accumulation of marrow fat in GR-CKO mice represents a defect in mechanisms of

BMAT lipolysis, as loss of GR function in extra-skeletal adipose depots promotes fat expansion in this manner [64] and Osx-Cre is active in bone marrow adipocytes [46]; analyses to address lipolytic mechanisms in GR-CKO BMAT are ongoing. Interestingly, whole-body percent fat mass also demonstrated a mild increase in constitutive GR-CKO mice, even though Osx-Cre is not active in fat depots outside the skeleton [46], raising questions of whether the skeletal phenotype may induce changes to global fat depots through cytokine release or altered hormonal signaling. It is intriguing that GR expression tended to be increased, rather than unchanged, in the gonadal white fat pad, skeletal muscle, and liver of the 21-month-old constitutive Osx-Cre:GR-CKO mice which also presented with a variety of extra-skeletal phenotypes. While we cannot rule out the contributions of developmental defects related to the use of Osx-Cre at this time, there is precedent for altered glucocorticoid signaling in one tissue affecting other body systems. For example, loss of GR expression in white adipose tissue (via adiponectin-Cre) impaired adipocyte lipolysis, leading to disproportionate breakdown of muscle tissue as an energy source during fasting, but protecting against liver steatosis in models of high fat feeding [65] and corticosterone treatment [64]. Whether the up-regulation of GR expression and phenotypic changes in the extra-skeletal tissues observed here reflects an artifact related to the Osx-Cre or true mechanisms of inter-organ crosstalk or systemic energy balance will be interrogated in future studies.

In another transgenic model of osteoporosis (Hdac3-CKO mice) previously reported by our group, BMAT accumulation was attributed in part to increased osteoblastic lipid storage that was driven by glucocorticoid signaling [33]. The *in vitro* data from the current study also showed GR-CKO osteoblasts to have increased propensity to store intracellular lipid droplets when treated with dexamethasone—despite insufficient expression of its classical glucocorticoid receptor—suggesting a potential compensatory mechanism. Because of this, our understanding of BMAT biology in the current model will benefit from further investigation of the osteogenic-adipogenic lineage commitment potential of GR-CKO progenitors. It has been reported that the MR can bind glucocorticoids with strong affinity to act on downstream glucocorticoid- or mineralocorticoid-responsive elements [57]. Our results indicated that MR inhibition reduced lipid storage in osteogenic cultures of GR-CKO cells, whereas GR inhibition with RU486 (mifepristone) exacerbated lipid accumulation. Importantly, increased MR activation is associated with cortical bone loss, metabolic dysfunction, increased adipogenesis and reactive oxygen species generation, and the induction of an inflammatory phenotype [66,67]. The highly energetic cellular phenotype of GR-CKO osteoblasts and the increased metabolic rate in GR-CKO mice in the current study could be consistent with the consequences of upregulated MR signaling, further supporting a potential role for the MR in mediating the deleterious effects of elevated glucocorticoids when GR function is suppressed. As such, future work will focus on determining the role of the MR in the current model through quantification of MR expression in this GR-CKO model and testing receptor blockade *in vivo* and *in vitro* using a potent MR antagonist such as eplerenone. The characterization of the inflammatory profile of GR-WT and GR-CKO mice is also a focus of our ongoing work, given the close relationships between glucocorticoid signaling through the GR and MR and alterations to

the circulating levels of inflammatory cytokines such as TNFα, IL-1β, and IL-6 in these pathways [24,68,69].

Of particular interest in the context of tissue crosstalk was the skeletal muscle phenotype of these animals, considering the finding that a constitutive Osx-targeted loss of GR function altered muscle mass across age groups. Specifically, whole-body percent lean mass was decreased in constitutive GR-CKO mice, and this phenotype was supported by histological analyses of muscle fiber size, which was also decreased in the slow-twitch soleus muscle of the constitutive GR-CKO animals. While it is difficult to separate the effects of reduced muscle mass from reduced overall body mass in the constitutive GR-CKO mice, as seen in the data for quadriceps mass, it is notable that percent lean mass measured by DXA was significantly lower in the constitutive GR-CKO mice despite already being corrected to overall body size (% lean mass = lean area / body area, excluding the head), at least raising the possibility that the effects on muscle are more than artifact. The lower muscle mass in the 21-month-old constitutive GR-CKO mice was associated with a significant decrease in voluntary physical activity, as aged constitutive GR-CKO mice exhibited reduced CLAMS cage ambulatory activity and voluntary wheel running. In contrast, previous work showed that muscle-specific loss of GR function contributed to muscle hypertrophy, though these muscle conditional knockout models induced systemic changes in other tissues [70,71]. Regardless, it is interesting that muscle-specific loss of GR function produced a positive effect on muscle mass, whereas the loss of GR in Osx-expressing cells led to decreased muscle mass, and a concomitant increase in GR mRNA expression in the tissue (Supplemental Figure S2C). Together with the current data, these findings raise the possibility of a bone-muscle crosstalk mechanism in the Osx-targeted GR-CKO model that should be considered in future work. However, we wish to clearly acknowledge the limitation that these analyses have thus far been confined to our constitutive GR-CKO model, and have not yet been repeated in the doxycycline-treated adult-onset GR-CKO mice. Moreover, we also wish to acknowledge the limitation that Osx-Cre+ control were not available as a control for our aging studies, but also note that any body size differences between WT Osx-Cre+ and WT Osx-Cre− littermates resolve by 12 weeks of age, whereas the majority of our muscle-centric studies were conducted at 6 months and 21 months of age [44]. Further investigation and additional analysis across age groups will be important for determining the effects of aging and GR function on any potential tissue crosstalk mechanisms between muscle and bone.

In conclusion, the findings from the current study suggest that GR function in Osx-expressing cells is important for healthy musculoskeletal aging and that compensatory glucocorticoid signaling mechanisms (such as those mediated by the MR) may function in the absence of the GR, further highlighting the complexities of glucocorticoid signaling in bone biology and discovering new avenues to identify potential therapeutic targets.

Supplementary Material

Refer to Web version on PubMed Central for supplementary material.

ACKNOWLEDGEMENTS

This work was supported by the NIH National Institute on Aging (grant number P01-AG036675; Project 4) and the American Diabetes Association (grant number 1-16-JDF-062). The authors would like to thank Dr. Louis Muglia for providing the GR-floxed mouse model. We thank Dr. Ismail Kaddour-Djebbar of the Charlie Norwood VA Medical Center for assistance with coordinating the Seahorse metabolic assays, and Dr. David Stepp and James Mintz for assistance with operating the CLAMS cages and obtaining metabolic measurements. We would like to acknowledge the Augusta University Electron Microscopy and Histology Core for tissue embedding and histological sectioning services. The contents of this article do not represent the views of the Department of Veterans Affairs or the United States Government.

Data availability statement:

The data that support the findings of this study are available from the corresponding author upon reasonable request.

References

1. Akkawi I, Zmerly H. Osteoporosis: Current Concepts. Joints. Jun 2018;6(2):122–7. Epub 2018/07/28. [PubMed: 30051110]
2. Rosen CJ. The Epidemiology and Pathogenesis of Osteoporosis. In: Feingold KR, Anawalt B, Boyce A, Chrousos G, de Herder WW, Dungan K, et al., editors. Endotext. South Dartmouth (MA)2000.
3. Kanis JA, Melton III LJ, Christiansen C, Johnston CC, Khaltaev N. The diagnosis of osteoporosis. J Bone Miner Res. 1994;9(8):1137–41. [PubMed: 7976495]
4. Nehlin JO, Jafari A, Tencerova M, Kassem M. Aging and lineage allocation changes of bone marrow skeletal (stromal) stem cells. Bone. Jun 2019;123:265–73. Epub 2019/04/05. [PubMed: 30946971]
5. Rosen CJ, Bouxsein ML. Mechanisms of disease: is osteoporosis the obesity of bone? Nat Clin Pract Rheumatol. Jan 2006;2(1):35–43. [PubMed: 16932650]
6. Yu B, Wang CY. Osteoporosis: The Result of an 'Aged' Bone Microenvironment. Trends Mol Med. Aug 2016;22(8):641–4. [PubMed: 27354328]
7. Fazeli PK, Horowitz MC, MacDougald OA, Scheller EL, Rodeheffer MS, Rosen CJ, et al. Marrow fat and bone--new perspectives. J Clin Endocrinol Metab. Mar 2013;98(3):935–45. [PubMed: 23393168]
8. Gorgey AS, Poarch HJ, Adler RA, Khalil RE, Gater DR. Femoral bone marrow adiposity and cortical bone cross-sectional areas in men with motor complete spinal cord injury. PM & R : the journal of injury, function, and rehabilitation. Nov 2013;5(11):939–48.
9. Scheller EL, Khoury B, Moller KL, Wee NK, Khandaker S, Kozloff KM, et al. Changes in Skeletal Integrity and Marrow Adiposity during High-Fat Diet and after Weight Loss. Front Endocrinol (Lausanne). 2016;7:102. [PubMed: 27512386]
10. Li J, Zhang N, Huang X, Xu J, Fernandes JC, Dai K, et al. Dexamethasone shifts bone marrow stromal cells from osteoblasts to adipocytes by C/EBPalpha promoter methylation. Cell death & disease. 2013;4:e832. [PubMed: 24091675]
11. Shen W, Chen J, Gantz M, Punyanitya M, Heymsfield SB, Gallagher D, et al. MRI-measured pelvic bone marrow adipose tissue is inversely related to DXA-measured bone mineral in younger and older adults. Eur J Clin Nutr. Sep 2012;66(9):983–8. Epub 2012/04/12. [PubMed: 22491495]
12. Almeida M, Kim HN, Han L, Zhou D, Thostenson J, Porter RM, et al. Increased marrow adipogenesis does not contribute to age-dependent appendicular bone loss in female mice. Aging Cell. Nov 2020;19(11):e13247. Epub 2020/10/14. [PubMed: 33048436]
13. Botolin S, McCabe LR. Inhibition of PPARgamma prevents type I diabetic bone marrow adiposity but not bone loss. Journal of cellular physiology. Dec 2006;209(3):967–76. [PubMed: 16972249]
14. Iwaniec UT, Turner RT. Failure to generate bone marrow adipocytes does not protect mice from ovariectomy-induced osteopenia. Bone. Mar 2013;53(1):145–53. [PubMed: 23246792]

15. Scheller EL, Rosen CJ. What's the matter with MAT? Marrow adipose tissue, metabolism, and skeletal health. Ann N Y Acad Sci. Apr 2014;1311:14–30. Epub 2014/03/22. [PubMed: 24650218]
16. Cao J, Ding K, Pan G, Rosario R, Su Y, Bao Y, et al. Deletion of PPARgamma in Mesenchymal Lineage Cells Protects Against Aging-Induced Cortical Bone Loss in Mice. J Gerontol A Biol Sci Med Sci. Apr 17 2020;75(5):826–34. Epub 2020/02/16. [PubMed: 32060555]
17. Ambrosi TH, Scialdone A, Graja A, Gohlke S, Jank AM, Bocian C, et al. Adipocyte Accumulation in the Bone Marrow during Obesity and Aging Impairs Stem Cell-Based Hematopoietic and Bone Regeneration. Cell Stem Cell. Jun 1 2017;20(6):771–84 e6. Epub 2017/03/24. [PubMed: 28330582]
18. Justesen J, Stenderup K, Ebbesen EN, Mosekilde L, Steiniche T, Kassem M. Adipocyte tissue volume in bone marrow is increased with aging and in patients with osteoporosis. Biogerontology. 2001;2:165–71. [PubMed: 11708718]
19. Rosen CJ, Ackert-Bicknell C, Rodriguez JP, Pino AM. Marrow fat and the bone microenvironment: developmental, functional, and pathological implications. Crit Rev Eukaryot Gene Expr. 2009;19(2):109–24. [PubMed: 19392647]
20. JafariNasabian P, Inglis JE, Reilly W, Kelly OJ, Ilich JZ. Aging human body: changes in bone, muscle and body fat with consequent changes in nutrient intake. Journal of Endocrinology. 2017;234:R37–R51. [PubMed: 28442508]
21. Deuschle M, Gotthardt U, Schweiger U, Weber B, Korner A, Schmider J, et al. With aging in humans the activity of the hypothalamus-pituitary-adrenal system increases and its diurnal amplitude flattens. Life Sciences. 1997;61(22):2239–46. [PubMed: 9393943]
22. Halberg F, Albrecht PG, Bittner JJ. Corticosterone rhythm of mouse adrenal in relation to serum corticosterone and sampling. Am J Physiol. 1959;197(5):1083–5. [PubMed: 14398943]
23. Kino T, Chrousos GP. Acetylation-mediated epigenetic regulation of glucocorticoid receptor activity: circadian rhythm-associated alterations of glucocorticoid actions in target tissues. Mol Cell Endocrinol. Apr 10 2011;336(1–2):23–30. Epub 2010/12/15. [PubMed: 21146585]
24. Almeida M, Han L, Ambrogini E, Weinstein RS, Manolagas SC. Glucocorticoids and tumor necrosis factor alpha increase oxidative stress and suppress Wnt protein signaling in osteoblasts. J Biol Chem. Dec 30 2011;286(52):44326–35. Epub 2011/10/28. [PubMed: 22030390]
25. Nixon M, Andrew R, Chapman KE. It takes two to tango: dimerisation of glucocorticoid receptor and its anti-inflammatory functions. Steroids. Jan 2013;78(1):59–68. Epub 2012/11/07. [PubMed: 23127816]
26. Lim HW, Uhlenhaut NH, Rauch A, Weiner J, Hubner S, Hubner N, et al. Genomic redistribution of GR monomers and dimers mediates transcriptional response to exogenous glucocorticoid in vivo. Genome Res. Jun 2015;25(6):836–44. Epub 2015/05/10. [PubMed: 25957148]
27. Hua G, Ganti KP, Chambon P. Glucocorticoid-induced tethered transrepression requires SUMOylation of GR and formation of a SUMO-SMRT/NCoR1-HDAC3 repressing complex. Proc Natl Acad Sci U S A. Feb 2 2016;113(5):E635–43. [PubMed: 26712006]
28. Hua G, Paulen L, Chambon P. GR SUMOylation and formation of an SUMO-SMRT/NCoR1-HDAC3 repressing complex is mandatory for GC-induced IR nGRE-mediated transrepression. Proc Natl Acad Sci U S A. Feb 2 2016;113(5):E626–34. [PubMed: 26712002]
29. Weinstein RS. Glucocorticoid-induced osteonecrosis. Endocrine. Apr 2012;41(2):183–90. Epub 2011/12/16.
30. Weinstein RS, Jilka RL, Parfitt AM, Manolagas SC. Inhibition of osteoblastogenesis and promotion of apoptosis of osteoblasts and osteocytes by glucocorticoids. J Clin Invest. 1998;102:274–82. [PubMed: 9664068]
31. Ishida Y, Heersche JNM. Glucocorticoid-induced osteoporosis: both in vivo and in vitro concentrations of glucocorticoids higher than physiological levels attenuate osteoblast differentiation. J Bone Miner Res. 1998;13(12).
32. Canalis E, Bilezikian JP, Angeli A, Giustina A. Perspectives on glucocorticoid-induced osteoporosis. Bone. Apr 2004;34(4):593–8. [PubMed: 15050888]
33. McGee-Lawrence ME, Carpio LR, Schulze RJ, Pierce JL, McNiven MA, Farr JN, et al. Hdac3 Deficiency Increases Marrow Adiposity and Induces Lipid Storage and Glucocorticoid Metabolism in Osteochondroprogenitor Cells. Journal of bone and mineral research : the official

journal of the American Society for Bone and Mineral Research. Jan 2016;31(1):116–28. [PubMed: 26211746]

34. O'Brien CA, Jia D, Plotkin LI, Bellido T, Powers CC, Stewart SA, et al. Glucocorticoids act directly on osteoblasts and osteocytes to induce their apoptosis and reduce bone formation and strength. Endocrinology. Research Support, U.S. Gov't, Non-P.H.S. Research Support, U.S. Gov't, P.H.S. Apr 2004;145(4):1835–41. Epub 2003/12/24. [PubMed: 14691012]
35. Weinstein RS, Wan C, Liu Q, Wang Y, Almeida M, O'Brien CA, et al. Endogenous glucocorticoids decrease skeletal angiogenesis, vascularity, hydration, and strength in aged mice. Aging cell. Research Support, N.I.H., Extramural Research Support, Non-U.S. Gov't Research Support, U.S. Gov't, Non-P.H.S. Apr 2010;9(2):147–61. Epub 2010/01/06. [PubMed: 20047574]
36. Henneicke H, Kim S, Swarbrick MM, Li J, Gasparini SJ, Thai J, et al. Skeletal glucocorticoid signalling determines leptin resistance and obesity in aging mice. Molecular metabolism. Oct 10 2020;42:101098. Epub 2020/10/13. [PubMed: 33045434]
37. Rauch A, Seitz S, Baschant U, Schilling AF, Illing A, Stride B, et al. Glucocorticoids suppress bone formation by attenuating osteoblast differentiation via the monomeric glucocorticoid receptor. Cell Metab. Jun 9 2010;11(6):517–31. Epub 2010/06/04. [PubMed: 20519123]
38. Pierce JL, Ding KH, Xu J, Sharma AK, Yu K, Del Mazo Arbona N, et al. The glucocorticoid receptor in osteoprogenitors regulates bone mass and marrow fat. J Endocrinol. Jul 1 2019. Epub 2019/08/02.
39. Kappel S, Hawkins P, Mendl MT. To Group or Not to Group? Good Practice for Housing Male Laboratory Mice. Animals (Basel). Nov 24 2017;7(12). Epub 2017/12/01.
40. Ackert-Bicknell CL, Anderson LC, Sheehan S, Hill WG, Chang B, Churchill GA, et al. Aging Research Using Mouse Models. Curr Protoc Mouse Biol. Jun 1 2015;5(2):95–133. Epub 2015/06/13. [PubMed: 26069080]
41. Brewer JA, Khor B, Vogt SK, Muglia LM, Fujiwara H, Haegele KE, et al. T-cell glucocorticoid receptor is required to suppress COX-2-mediated lethal immune activation. Nat Med. Oct 2003;9(10):1318–22. Epub 2003/09/02. [PubMed: 12949501]
42. Kim HJ, Zhao H, Kitaura H, Bhattacharyya S, Brewer JA, Muglia LJ, et al. Glucocorticoids suppress bone formation via the osteoclast. J Clin Invest. Aug 2006;116(8):2152–60. Epub 2006/08/01. [PubMed: 16878176]
43. Mittelstadt PR, Ashwell JD. Disruption of glucocorticoid receptor exon 2 yields a ligand-responsive C-terminal fragment that regulates gene expression. Mol Endocrinol. Aug 2003;17(8):1534–42. Epub 2003/05/17. [PubMed: 12750452]
44. Davey RA, Clarke M, Sastra S, Skinner J, Chiang C, Anderson PH, et al. Decreased body weight in young Osterix-Cre transgenic mice results in delayed cortical bone expansion and accrual. Transgenic Res. 2012;21(4):885–93. [PubMed: 22160436]
45. Wang L, Mishina Y, Liu F. Osterix-Cre transgene causes craniofacial bone development defect. Calcified tissue international. Feb 2015;96(2):129–37. [PubMed: 25550101]
46. Chen J, Shi Y, Regan J, Karuppaiah K, Ornitz DM, Long F. Osx-Cre targets multiple cell types besides osteoblast lineage in postnatal mice. PloS one. Research Support, N.I.H., Extramural Research Support, Non-U.S. Gov't 2014;9(1):e85161. Epub 2014/01/24. [PubMed: 24454809]
47. Huang W, Olsen BR. Skeletal defects in Osterix-Cre transgenic mice. Transgenic Res. Feb 2015;24(1):167–72. Epub 2014/08/21. [PubMed: 25139670]
48. Rodda SJ, McMahon AP. Distinct roles for Hedgehog and canonical Wnt signaling in specification, differentiation and maintenance of osteoblast progenitors. Development. Aug 2006;133(16):3231–44. [PubMed: 16854976]
49. Marquardt N, Feja M, Hunigen H, Plendl J, Menken L, Fink H, et al. Euthanasia of laboratory mice: Are isoflurane and sevoflurane real alternatives to carbon dioxide? PloS one. 2018;13(9):e0203793. Epub 2018/09/11. [PubMed: 30199551]
50. Sapolsky RM, Romero LM, Munck AU. How do glucocorticoids influence stress responses? Integrating permissive, suppressive, stimulatory, and preparative actions. Endocr Rev. Feb 2000;21(1):55–89. Epub 2000/03/04. [PubMed: 10696570]

51. Boivin GP, Hickman DL, Creamer-Hente MA, Pritchett-Corning KR, Bratcher NA. Review of CO(2) as a Euthanasia Agent for Laboratory Rats and Mice. J Am Assoc Lab Anim Sci. Sep 1 2017;56(5):491–9. Epub 2017/09/15. [PubMed: 28903819]
52. Razidlo DF, Whitney TJ, Casper ME, McGee-Lawrence ME, Stensgard BA, Li X, et al. Histone deacetylase 3 depletion in osteo/chondroprogenitor cells decreases bone density and increases marrow fat. PloS one. Research Support, N.I.H., Extramural Research Support, Non-U.S. Gov't 2010;5(7):e11492. Epub 2010/07/16. [PubMed: 20628553]
53. Cawthorn WP, Scheller EL, Parlee SD, Pham HA, Learman BS, Redshaw CM, et al. Expansion of Bone Marrow Adipose Tissue During Caloric Restriction Is Associated With Increased Circulating Glucocorticoids and Not With Hypoleptinemia. Endocrinology. Feb 2016;157(2):508–21. Epub 2015/12/24. [PubMed: 26696121]
54. Pierce JL, Begun DL, McGee-Lawrence ME, Westendorf JJ. Defining osteoblast and adipocyte lineages in the bone marrow. Bone. 2019;118:2–7. [PubMed: 29782940]
55. McGee-Lawrence ME, White TA, LeBrasseur NK, Westendorf JJ. Conditional deletion of Hdac3 in osteoprogenitor cells attenuates diet-induced systemic metabolic dysfunction. Molecular and cellular endocrinology. Jul 15 2015;410:42–51. [PubMed: 25666992]
56. McGee-Lawrence ME, Pierce JL, Yu K, Culpepper NR, Bradley EW, Westendorf JJ. Loss of Hdac3 in osteoprogenitors increases bone expression of osteoprotegerin, improving systemic insulin sensitivity. Journal of cellular physiology. Apr 2018;233(4):2671–80. Epub 2017/08/26. [PubMed: 28840938]
57. Fumoto T, Ishii KA, Ito M, Berger S, Schutz G, Ikeda K. Mineralocorticoid receptor function in bone metabolism and its role in glucocorticoid-induced osteopenia. Biochemical and biophysical research communications. May 9 2014;447(3):407–12. Epub 2014/04/10. [PubMed: 24713303]
58. Pierce JL, Roberts RL, Yu K, Kendall RK, Kaiser H, Davis C, et al. Kynurenine suppresses osteoblastic cell energetics in vitro and osteoblast numbers in vivo. Exp Gerontol. Feb 2020;130:110818. Epub 2019/12/22. [PubMed: 31862422]
59. Zhang Y, Marsboom G, Toth PT, Rehman J. Mitochondrial respiration regulates adipogenic differentiation of human mesenchymal stem cells. PLoS One. 2013;8(10):e77077. Epub 2013/11/10. [PubMed: 24204740]
60. Guntur AR, Gerencser AA, P TL, DeMambro VE, Bornstein SA, Mookerjee SA, et al. Osteoblast like MC3T3-E1 cells prefer glycolysis for ATP production but adipocyte like 3T3-L1 cells prefer oxidative phosphorylation. J Bone Miner Res. Jan 17 2018. Epub 2018/01/18.
61. Chen C, Shih YV, Kuo T, Lee OK, Wei Y. Coordinated changes of mitochondrial biogenesis and antioxidant enzymes during osteogenic differentiation of human mesenchymal stem cells. Stem Cells. 2008;26:960–8. [PubMed: 18218821]
62. Iwaniec UT, Dube MG, Boghossian S, Song H, Helferich WG, Turner RT, et al. Body mass influences cortical bone mass independent of leptin signaling. Bone. Mar 2009;44(3):404–12. Epub 2008/12/20. [PubMed: 19095090]
63. Henneicke H, Kim S, Swarbrick MM, Li J, Gasparini SJ, Thai J, et al. Skeletal glucocortioid signaling determines leptin resistance and obesity in aging mice. Mol Met. 2020;42.
64. Dalle H, Garcia M, Antoine B, Boehm V, Do TTH, Buyse M, et al. Adipocyte Glucocorticoid Receptor Deficiency Promotes Adipose Tissue Expandability and Improves the Metabolic Profile Under Corticosterone Exposure. Diabetes. Feb 2019;68(2):305–17. Epub 2018/11/21. [PubMed: 30455377]
65. Mueller KM, Hartmann K, Kaltenecker D, Vettorazzi S, Bauer M, Mauser L, et al. Adipocyte Glucocorticoid Receptor Deficiency Attenuates Aging- and HFD-Induced Obesity and Impairs the Feeding-Fasting Transition. Diabetes. Feb 2017;66(2):272–86. Epub 2016/09/22. [PubMed: 27650854]
66. Hirata A, Maeda N, Hiuge A, Hibuse T, Fujita K, Okada T, et al. Blockade of mineralocorticoid receptor reverses adipocyte dysfunction and insulin resistance in obese mice. Cardiovasc Res. Oct 1 2009;84(1):164–72. Epub 2009/06/10. [PubMed: 19505930]
67. Hirata A, Maeda N, Nakatsuji H, Hiuge-Shimizu A, Okada T, Funahashi T, et al. Contribution of glucocorticoid-mineralocorticoid receptor pathway on the obesity-related adipocyte dysfunction.

Biochemical and biophysical research communications. Mar 9 2012;419(2):182–7. Epub 2012/02/14. [PubMed: 22326264]

68. Ahasan MM, Hardy R, Jones C, Kaur K, Nanus D, Juarez M, et al. Inflammatory regulation of glucocorticoid metabolism in mesenchymal stromal cells. Arthritis Rheum. Jul 2012;64(7):2404–13. [PubMed: 22294469]
69. Cooper MS, Bujalska IJ, Rabbitt EH, Walker EA, Bland R, Sheppard MC, et al. Modulation of 11B-Hydroxysteroid Dehydrogenase Isozymes by Proinflammatory Cytokines in Osteoblasts: An Autocrine Switch from Glucocorticoid Inactivation to Activation. J Bone Miner Res. 2001;16(6).
70. Shimizu N, Maruyama T, Yoshikawa N, Matsumiya R, Ma Y, Ito N, et al. A muscle-liver-fat signalling axis is essential for central control of adaptive adipose remodelling. Nat Commun. Apr 1 2015;6:6693. Epub 2015/04/02. [PubMed: 25827749]
71. de Theije CC, Schols A, Lamers WH, Ceelen JJM, van Gorp RH, Hermans JJR, et al. Glucocorticoid Receptor Signaling Impairs Protein Turnover Regulation in Hypoxia-Induced Muscle Atrophy in Male Mice. Endocrinology. Jan 1 2018;159(1):519–34. Epub 2017/10/27. [PubMed: 29069356]

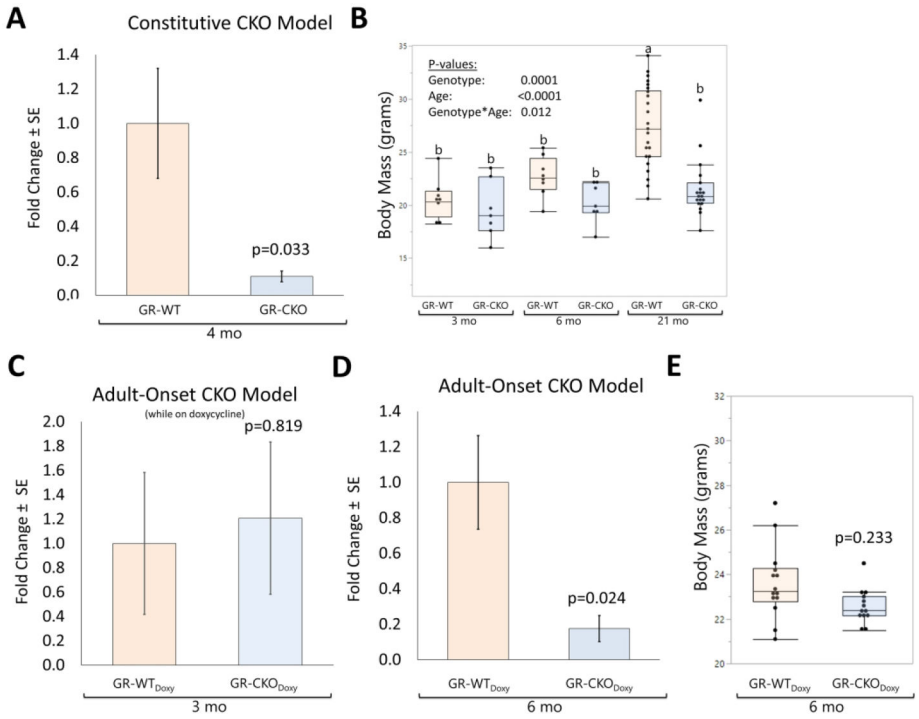

Figure 1: Validation of GR-CKO in bone.

(A) RT-qPCR analysis of the glucocorticoid receptor (GR) exon 2 in cortical bone samples from young female (4 months) constitutive GR-WT and GR-CKO (n=4) mice maintained on a regular diet. (B) Body mass (in grams) of constitutive GR-CKO and GR-WT littermates at 3, 6, or 21 months of age. Bars with different superscript letters are significantly ($p<0.05$) different from one another. (C) Expression levels of the GR in cortical bone from adult-onset GR-WT and GR-CKO mice (n=3) maintained on a doxycycline diet for 3 months until sacrifice (i.e., mice remained on doxycycline until sacrifice). (D) GR expression levels in cortical bone from 6-month-old GR-WT and GR-CKO mice (n=4) that were subjected to a doxycycline diet for 3 months followed by a 3 month recovery period on a regular diet with no doxycycline to permit Cre expression. (E) Body mass (in grams) of female adult onset GR-WT and GR-CKO mice at 6 months of age, 3 months after cessation of the doxycycline diet. Boxes show median, quartiles and outlier fences for each dataset, whereas bar charts show group mean +/− SEM. Each data point represents one mouse.

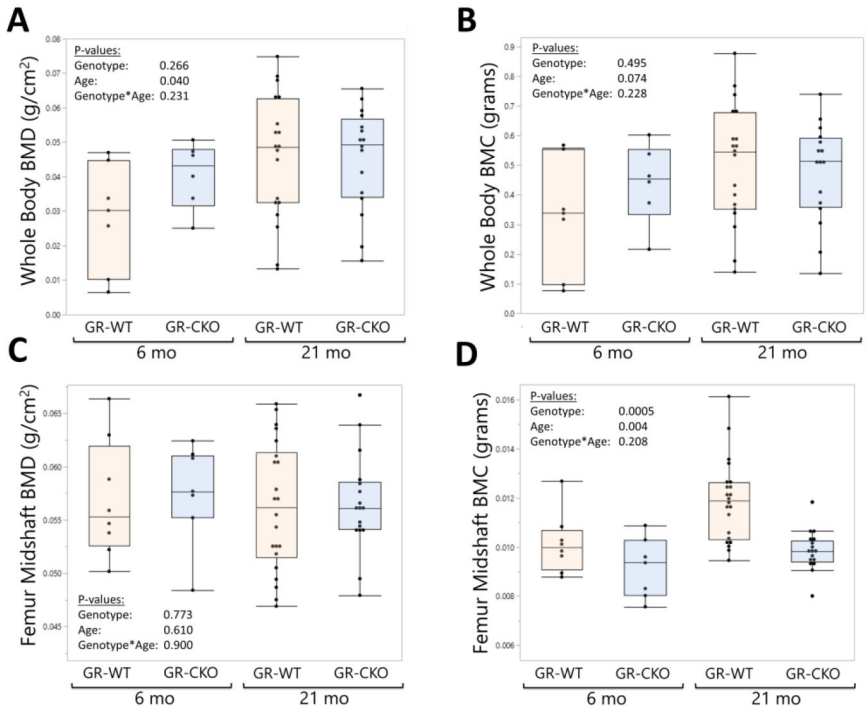

Figure 2: Conditional deletion of the glucocorticoid receptor had minimal impact on bone mineral density as measured by DXA.

Dual X-Ray absorptiometry (DXA; Kubtec Digimus) analyses of constitutive GR-WT and GR-CKO female mice were quantified at 6- and 21 months of age for (A) whole body bone mineral density (BMD), (B) whole body bone mineral content (BMC, grams), (C) femur midshaft BMD, and (D) femur midshaft BMC. Boxes show median, quartiles and outlier fences for each dataset. Each data point represents one mouse.

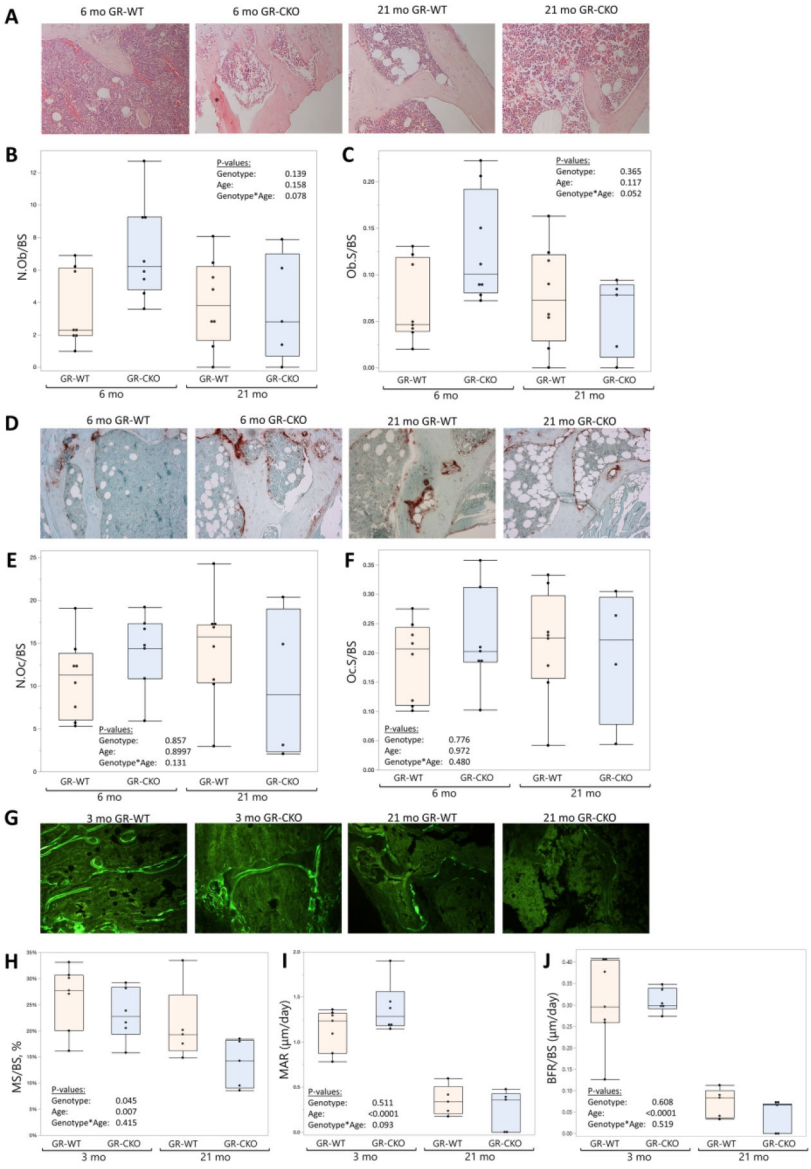

Figure 3: The low bone mass phenotype of GR-CKO mice was associated with decreased trabecular bone mineralization with age.

(A) Representative H&E-stained tibiae from constitutive GR-WT and GR-CKO mice at 6- and 21 months of age. (B) Osteoblast number (N.Ob/BS) and (C) osteoblast surface (Ob.S/BS) were quantified in the H&E-stained sections. (D) Representative tartrate-resistant acid phosphatase (TRAP)-stained tibial sections from constitutive GR-WT and GR-CKO mice at 6- and 21 months of age. (E) Osteoclast number (N.Oc/BS) and (F) osteoclast surface (Oc.S/BS) were quantified in sections labeled by TRAP staining (G) Representative images of calcein-labeled bone in constitutive GR-WT and GR-CKO femur sections at 3- and 21-months of age. (H) Percent mineralizing surface (MS/BS, %), (I) mineral apposition rate (MAR, µm/day), and (J) bone formation rate (BFR/BS, µm/day) were calculated from single- and double-labeled surfaces in the sections. Boxes show median, quartiles and outlier fences for each dataset. Each data point represents one mouse.

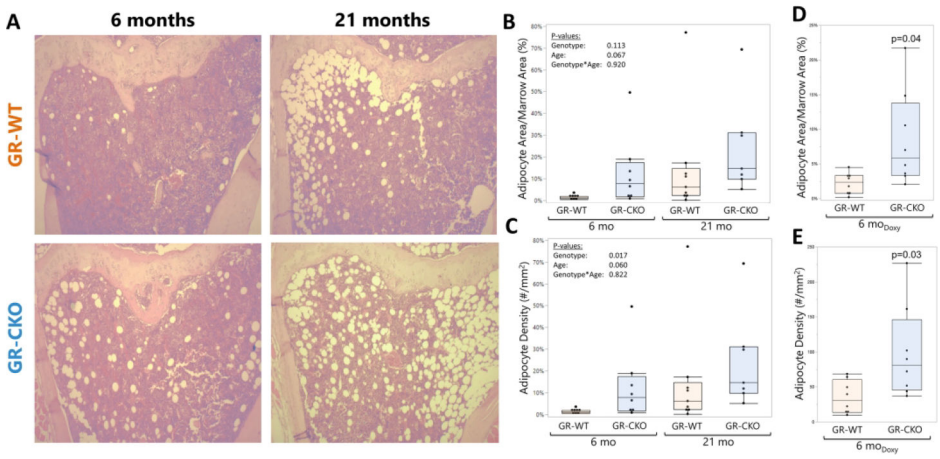

Figure 4: GR-CKO mice accumulate increased bone marrow fat that persists with aging

(A) Representative images for H&E-stained tibial sections from constitutive GR-WT and GR-CKO mice at 6- and 21 months of age. Quantification of (B) adipocyte area fraction (Ad.Ar/M.Ar, %) and (C) adipocyte density (#/mm^2) of the proximal tibiae in the constitutive GR-CKO and WT mice was performed using Bioquant Osteo. (D) Adipocyte area fraction and (E) adipocyte density were also quantified in the proximal tibiae of the 6-month-old adult-onset GR-CKO and GR-WT mice (3 months of doxycycline diet followed by 3 months of normal diet to induce Cre expression). Boxes show median, quartiles and outlier fences for each dataset. Each data point represents one mouse.

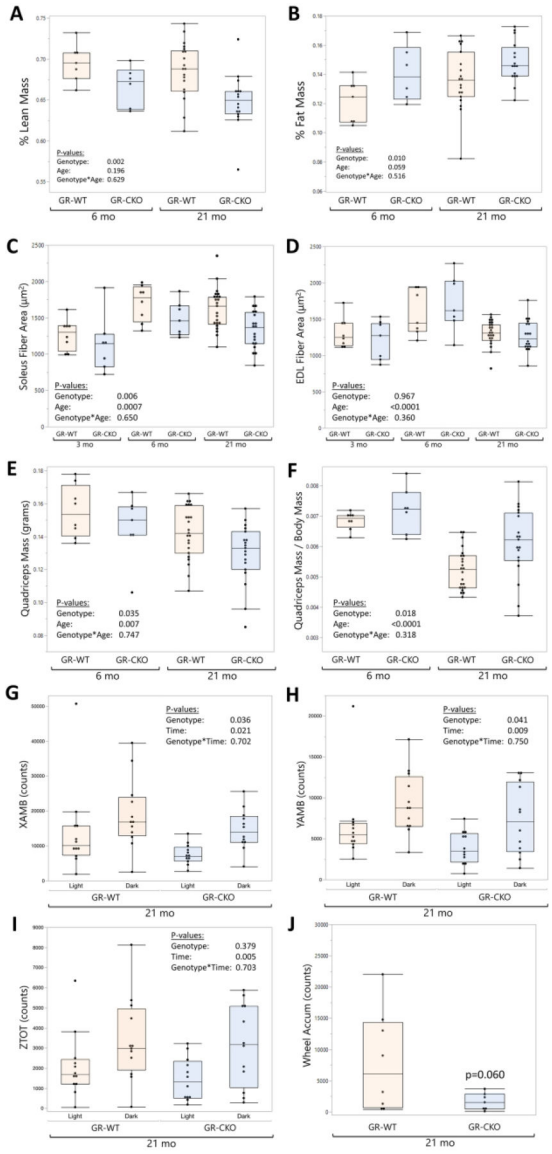

Figure 5: Loss of GR function in Osx-expressing cells alters skeletal muscle mass and reduces physical activity.

Dual X-Ray absorptiometry (DXA; Kubtec Digimus) analyses of constitutive GR-WT and GR-CKO female mice were quantified at 6- and 21 months of age for (A) whole body percent lean mass (lean area / total body area, excluding the head) and (B) whole body percent fat mass (fat area / total body area, excluding the head). Average muscle fiber areas for the (C) Soleus and (D) EDL were quantified in the constitutive GR-CKO or GR-WT littermate mice at 3, 6, or 21 months of age. E-F) Quadriceps muscles were removed at sacrifice and weighed on an electronic balance; data are presented in terms of absolute mass (E) or quadriceps mass normalized to body mass. G-I) Comprehensive laboratory animal monitoring system (CLAMS) quantification of cage ambulatory movement across the (G) x-axis and (H) y-axis, and total counts of rearing up across the (I) z-axis shown for 21-month-old constitutive GR-WT and GR-CKO mice during 12-hour light and dark periods. (J) Voluntary wheel running counts for 21-month-old constitutive GR-WT and

GR-CKO mice accumulated over a 5-day period. Boxes show median, quartiles and outlier fences for each dataset. Each data point represents one mouse.

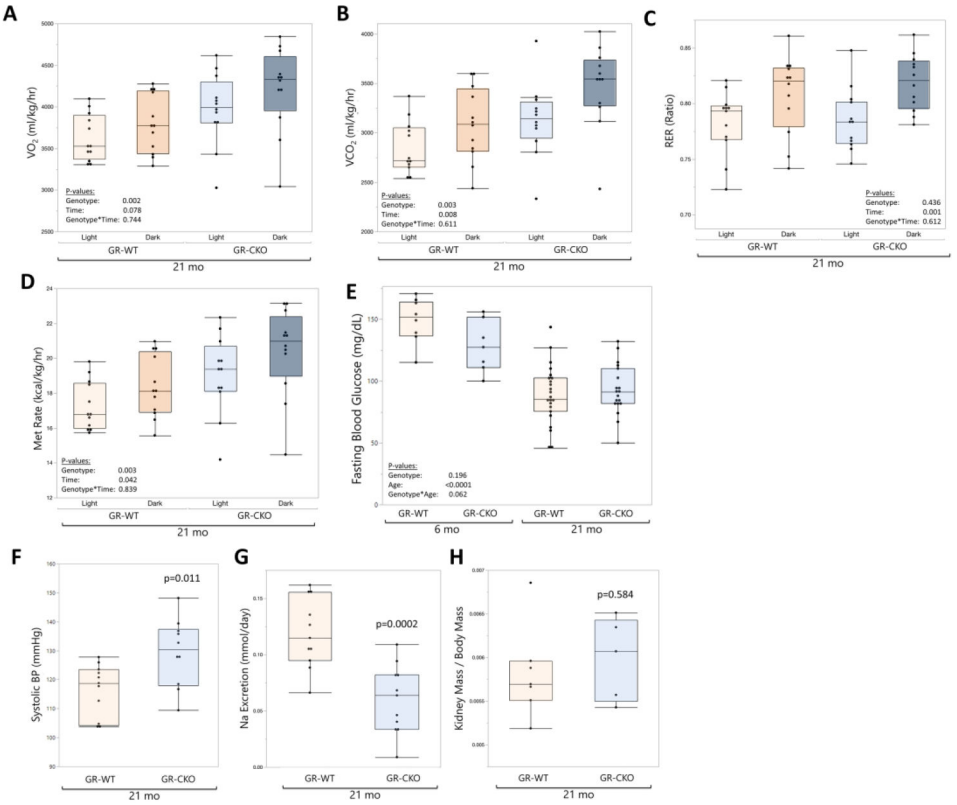

Figure 6: GR deficiency in Osx-expressing cells is associated with systemic metabolic dysfunction.

CLAMS measurements of (A) oxygen consumption (mL/kg/hr), (B) carbon dioxide production (mL/kg/hr), (C) respiratory exchange ratio (of O_2 versus CO_2), and (D) metabolic rate (kcal/kg/hr; kcal body heat produced per hour, normalized to body mass) were collected for the constitutive GR-CKO and GR-WT littermates at 21 months of age during 12-hour light and dark periods. (E) Fasting (6 hour) blood glucose measurements of the constitutive GR-CKO and GR-WT mice were collected at 6- and 21-months of age with a handheld glucometer. (F) Systolic blood pressure (mmHg) was quantified from tail cuff blood pressure measurements in constitutive GR-WT and GR-CKO mice at 21 months of age. (G) Urine sodium excretion (nmol/day) measured from constitutive GR-CKO and GR-WT mice mice housed in metabolic cages. (H) Kidney weights normalized to body mass for constitutive GR-WT and GR-CKO at 21 months of age. Boxes show median, quartiles and outlier fences for each dataset. Each data point represents one mouse.

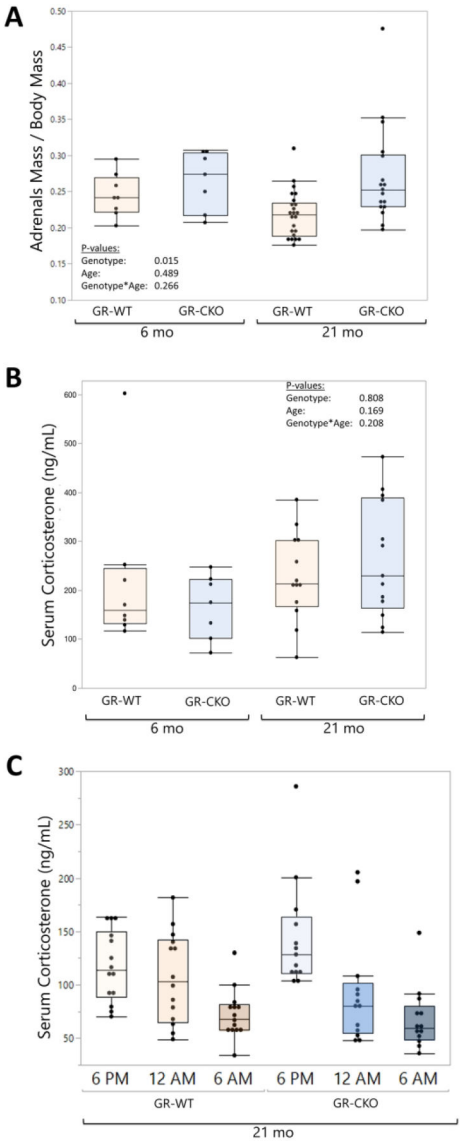

Figure 7: GR-CKO in Osx-expressing cells affected normalized adrenal mass.

(A) Paired adrenal weights (in grams) were measured and normalized to body mass in constitutive GR-WT and GR-CKO mice at 6- or 21 months of age. (B) Serum corticosterone (ng/mL) levels were measured by ELISA on constitutive GR-WT and GR-CKO sera harvested at sacrifice at 6- or 21 months of age. (C) Corticosterone ELISA results from constitutive GR-WT and GR-CKO sera harvested at 21 months of age by non-terminal tail bleeds at 6:00 p.m., 12:00 a.m., and 6:00 a.m. with a rest period of at least 3 days between blood collection cycles.

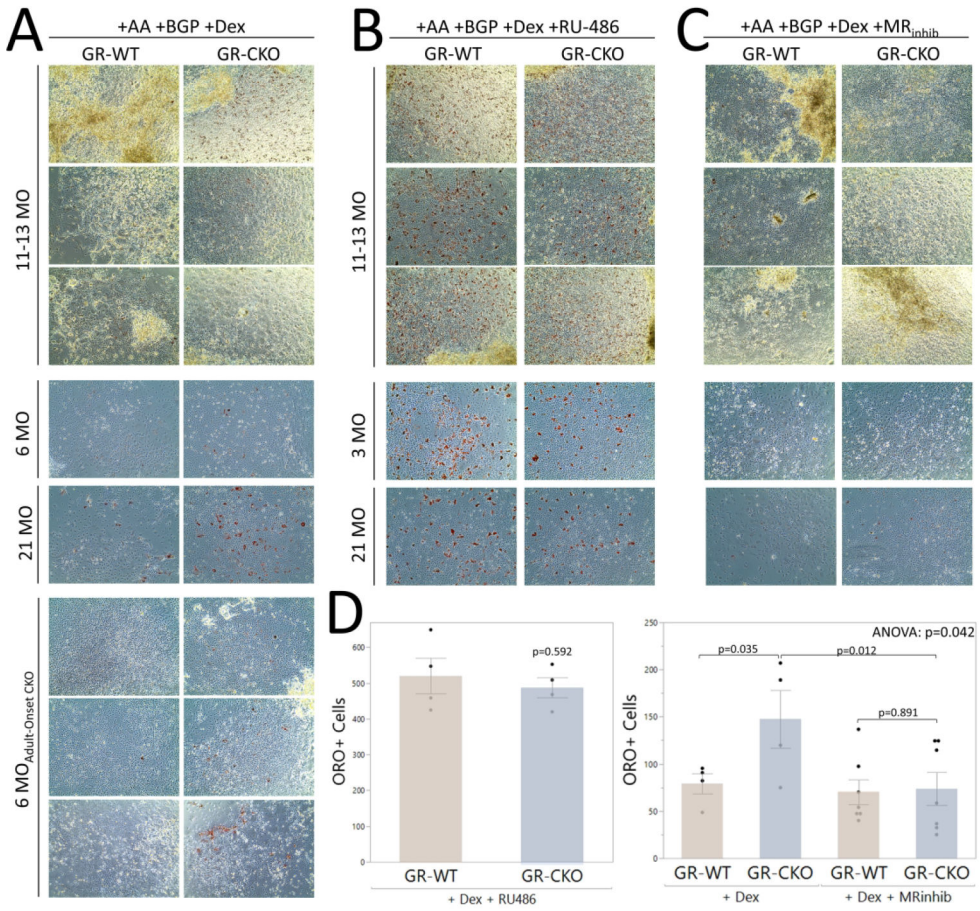

Figure 8: GR-CKO or pharmacological GR inhibition induces lipid droplet accumulation in osteogenic cultures that is abrogated by MR antagonist treatment.

BMSC-derived osteoblasts were obtained by pooling age- and genotype-matched bone marrow stromal cells for culture in osteogenic induction medium. After 21 days in culture, osteoblasts were stained with 60% Oil Red O for visualization of intracellular lipid droplets. Microscopic images were obtained at 10X magnification and represent a minimum of three technical replicates (wells) per genotype. For each culture condition, each row of images is representative of a separate biological replicate (i.e., separate batch of animals). A) GR-CKO osteoblasts consistently stored more lipid droplets than GR-WT osteoblasts across three biological replicates (separate batches of animals) of cells from constitutive GR-CKO and GR-WT mice sacrificed at 11–13 months of age, 1 biological replicate of constitutive GR-CKO and GR-WT mice at 6 months or 21 months of age, and three biological replicates of the adult-onset (doxycycline-treated) GR-CKO and WT mice at 6 months of age. B) When treated with the GR-antagonist RU-486, lipid storage was abundant and comparable between constitutive GR-CKO and GR-WT osteoblast cultures. However, in the presence of mineralocorticoid receptor antagonists (spironolactone or eplerenone), lipid storage in the GR-CKO osteoblast cultures was reduced. D) The number of Oil Red O-stained cells was quantified from each biological replicate of the constitutive GR-CKO cultures. Boxes

show median, quartiles and outlier fences for each dataset. Each data point represents one biological replicate. P-values for pairwise comparisons are shown.

Table 1:

MicroCT parameters of constitutive GR-CKO and GR-WT bone at 3 months and 21 months of age

Parameter	Mean ± SE				$p_{genotype}$	p_{age}	$p_{genotype \times age\ interaction}$
Ct. T.Ar (mm^2)	1.687 ± 0.060[b]	1.635 ± 0.062[b]	1.986 ± 0.017[a]	1.661 ± 0.034[b]	0.0008	0.003	0.010
Ct. B.Ar (mm^2)	0.658 ± 0.019[b]	0.628 ± 0.026[b]	0.783 ± 0.019[a]	0.627 ± 0.019[b]	0.0002	0.008	0.007
Ct. M.Ar (mm^2)	1.029 ± 0.044	1.007 ± 0.038	1.203 ± 0.013	1.034 ± 0.042	0.019	0.014	0.065
Ct. BV/TV	0.391 ± 0.006	0.384 ± 0.006	0.394 ± 0.008	0.379 ± 0.015	0.245	0.902	0.652
Ct. Imax (mm^4)	0.199 ± 0.013[ab]	0.180 ± 0.015[b]	0.240 ± 0.007[a]	0.164 ± 0.006[b]	0.0002	0.268	0.015
Ct. Imin(mm^4)	0.101 ± 0.007[b]	0.097 ± 0.008[b]	0.160 ± 0.007[a]	0.108 ± 0.003[b]	0.0003	<0.0001	0.002
Ct.Th (mm)	0.145 ± 0.003	0.140 ± 0.004	0.161 ± 0.004	0.141 ± 0.006	0.006	0.036	0.077
Ct. TBMD (mg/cm^3)	1.146 ± 0.012	1.106 ± 0.010	1.232 ± 0.008	1.200 ± 0.009	0.002	<0.0001	0.677
Tb.BV/TV	6.218 ± 0.595	4.342 ± 0.950	1.829 ± 1.477	0.078 ± 0.058	0.050	<0.0001	0.944
Tb.Th (mm)	0.046 ± 0.002	0.045 ± 0.001	0.042 ± 0.006	0.030 ± 0.005	0.078	0.019	0.126
Tb.N (1/mm)	1.373 ± 0.145	0.956 ± 0.204	0.438 ± 0.356	0.019 ± 0.012	0.052	0.0001	0.997
Tb.Sp (mm)	0.268 ± 0.018	0.328 ± 0.023	0.436 ± 0.019	0.461 ± 0.001	0.022	<0.0001	0.325
	3 mo GR-WT n=7	**3 mo GR-CKO n=7**	**21 mo GR-WT n=6**	**21 mo GR-CKO n=7**			

Parameter means and standard errors (SE) are presented. P-values for variables and interactions assessed by two-factor analysis of variance (ANOVA) are shown. For properties where a significant interaction was detected between genotype and age, group means with different superscript letters are significantly ($p<0.05$) different from one another, as indicated by Tukey-Kramer HSD post-hoc testing.

Table 2:

MicroCT parameters of adult-onset GR-CKO and GR-WT bone at 6 months of age

Parameter	Mean ± SE		p-value
Ct. T.Ar (mm^2)	1.703 ± 0.033	1.687 ± 0.044	0.784
Ct. B.Ar (mm^2)	0.718 ± 0.013	0.670 ± 0.007	0.005
Ct. M.Ar (mm^2)	0.985 ± 0.027	1.017 ± 0.040	0.527
Ct. B.Ar/T.Ar	0.422 ± 0.007	0.398 ± 0.008	0.055
Ct. Imax (mm^4)	0.207 ± 0.008	0.205 ± 0.009	0.856
Ct. Imin (mm^4)	0.111 ± 0.004	0.100 ± 0.005	0.105
Ct.Th (mm)	0.148 ± 0.003	0.134 ± 0.003	0.007
Ct. TBMD (mg/cm^3)	1.793± 0.008	1.775 ± 0.009	0.158
Tb.BV/TV	5.101 ± 0.200	2.874 ± 0.360	0.0007
Tb.Th (mm)	0.060 ± 0.007	0.040 ± 0.002	0.011
Tb.N (1/mm)	0.895 ± 0.089	0.741 ± 0.118	0.359
Tb.Sp (mm)	0.287 ± 0.063	0.224 ± 0.050	0.455
	6 mo GR-WT_{Doxy} n=6	**6 mo GR-CKO_{Doxy} n=7**	

Parameter means and standard errors (SE) are presented. P-values calculated by Student's t-test are shown.